


<https://doi.org/10.1590/2318-0331.282320230041>

Dam safety in Sergipe: Jacarecica I and Jacarecica II hypothetical cascade dam-break simulation

Segurança de barragens em Sergipe: simulação do rompimento hipotético em cascata das barragens Jacarecica I e Jacarecica II

Leonardo de Carvalho Souza Santa Rita¹ , Abraão Nunes de Oliveira¹ , André Quintão de Almeida¹  & Ludmilson Abritta Mendes¹ 

¹Universidade Federal de Sergipe, São Cristóvão, SE, Brasil

E-mails: leocarvalhossr@gmail.com (LCSSR), abraaooliveira435@gmail.com (ANO), andreqa@gmail.com (AQA), lamendes@academico.ufs.br (LAM)

Received: April 20, 2023 - Revised August 6, 2023 - Accepted: September 01, 2023

ABSTRACT

Despite of benefits such as water security and energy supply dams provide, there are environmental impacts and risks of accidents associated with their usage, i.e. rupture. In these cases, a structured Emergency Action Plan (EAP) must be executed to mitigate impacts and loss of life. To do so, hypothetical dam break scenarios must be simulated to obtain the flood's spatial coverage in downstream valley. In this regard, this work aimed to obtain the flood maps due to hypothetical ruptures of Jacarecica I and Jacarecica II dams (state of Sergipe), structures that don't have Safety Plans elaborated. HEC-RAS 2D model was used to elaborate flood inundation maps and assess hydrodynamic results, that showed the breach wave impacts residential, industrial and agricultural areas before reaching the city of Riachuelo, with high depths and velocities, and minimum arrival times of 6 hours. With rural and urban areas at risk, it is mandatory, according to the PNSB, that the dams' EAPs are prepared.

Keywords: Cascade dam failure; Dam safety plan; HEC-RAS; Inundation map; Hydrodynamic modelling.

RESUMO

Apesar de benefícios como segurança hídrica e fornecimento de energia que barragens garantem, há impactos ambientais e riscos de acidentes associados ao seu uso, como o rompimento. Nesses casos, um Plano de Ação de Emergência (PAE) estruturado deve ser executado para mitigar os impactos ambientais e a perda de vidas. Para tanto, cenários hipotéticos de rompimento devem ser simulados para obter a mancha de inundação no vale a jusante. Nesse sentido, este trabalho teve como objetivo obter a mancha de inundação da ruptura hipotética das barragens Jacarecica I e Jacarecica II (estado de Sergipe), estruturas que não possuem Planos de Segurança elaborados. O modelo 2D HEC-RAS foi utilizado para elaborar as manchas de inundação e avaliar os resultados hidrodinâmicos, que mostraram que a onda de ruptura impacta áreas residenciais, industriais e agrícolas antes de atingir a cidade de Riachuelo, com altas profundidades e velocidades, e tempos de chegada mínimos de 6 horas. Com áreas rurais e urbanas em risco, é obrigatório, segundo a PNSB, que os PAEs das barragens sejam elaborados.

Palavras-chave: Rompimento de barragem em cascata; Plano de segurança de barragem; HEC-RAS; Mapa de inundação; Modelagem hidrodinâmica.

INTRODUCTION

The construction of water infrastructure, such as dams, has been the solution traditionally used to satisfactorily meet the multiple uses of water. Although they occur with reduced frequency, isolated or cascade ruptures of these structures can cause disastrous consequences such as damage to properties, loss of life and profound changes in the environmental, social and economic scenarios (Hu et al., 2020; Armada, 2021; Guimarães et al., 2022; Ge et al., 2022).

After a relative delay in relation to the dam safety legislation worldwide, Brazil enacted in September 20, 2010, Law n. 12,334, establishing the National Dam Safety Policy (NDSP), which laid out objectives, foundations, instruments and competences to guide the prevention and response to accidents in dams with certain characteristics. In 2020, the Law n. 14,666 brought updates to the NDSP, improving dam safety management in Brazil (Guimarães et al., 2022).

According to Brazil's NDSP, the classification of dams is made by risk category (RC) and associated potential damage (APD). The first criteria depends on the technical characteristics, construction methods, state of conservation and age of the project and compliance with the Dam Safety Plan (DSP). The APD classification relies on the potential loss of human life and the economic, social and environmental impacts arising from the dam rupture.

For dams classified with high associated potential damage (APD), the legislation obliges entrepreneurs to prepare the Emergency Action Plan (EAP), a document that is part of the Dam Safety Plan (DSP) that establishes a set of actions to be carried out in case of emergencies such as ruptures or operational failures and that must be available in the enterprise, at the municipalities of the cities involved, and also to Civil Defense bodies.

Enterprises that still do not have safety management implemented as required by the NDSP are present in several Brazilian states. An example is the state of Sergipe, which has legislation still under development. Even with the support of Águas de Sergipe and PROGESTÃO - state and federal programs, respectively, that support water resources management in Sergipe -, there are no DSPs or EAPs implemented, which would be mandatory in some Sergipe dams, due to their classification in high APD (Agência Nacional de Águas e Saneamento Básico, 2021).

Allowing the implementation of the federal legislation instruments on dam safety management, such as the DSP and the EAP, the dam break models simulate the propagation of the flood wave in the downstream valleys. Through the inundation maps, obtained with the application of different failure scenarios, risk zoning can be performed, determining, for instance, the extension of the Self-Rescue Zone (SRZ), area where it is considered that, when emergency takes place, the people within must be able to guarantee its own ways of survival, without help from governmental authorities.

Different types of studies can be carried out by the models that perform flood wave propagation such as reservoir operation and urban flood modelling (Garcia et al., 2020), hazard zoning (Vieira et al., 2019; Ongdas et al., 2020), dam break uncertainty and risk assessment (Tschiedel & Paiva, 2018; Bellos et al., 2020; Tschiedel et al., 2020), cascade dam failure (Hu et al., 2020; Campos et al., 2020; Amini et al., 2022), sensitivity analyzes (Garoosi et al., 2022; Álvarez et al., 2017), and others.

Related to this work, hypothetical dam break studies are fundamental for establishing impacted areas and, thus, emergency actions plans.

Considering the need to develop DSPs for some dams in Sergipe and the absence of these documents, this work aimed to simulate the hydrodynamic effects in the downstream valleys of Jacarecica I and Jacarecica II dams due to their cascade hypothetical ruptures. Using HEC-RAS 2D hydrodynamic model, it was intended to map the inundation boundaries to subsidize the hydrological studies necessary for the elaboration of the EAP of the Jacarecica I and Jacarecica II dams, both located in the central portion of Sergipe's Agreste region and classified as high APD (Agência Nacional de Águas e Saneamento Básico, 2021). Furthermore, the HEC-RAS results were compared to the application of the National Water and Basic Sanitation Agency's Simplified Methodology elaborated for Jacarecica II dam (Fernandes et al., 2021).

MATERIALS AND METHODS

This work analyzed the hydrodynamic effects of Jacarecica I and Jacarecica II dams' hypothetical failure onto downstream valleys. Most probable (typical operation) and extreme (worsening in breach parameters) rupture scenarios were proposed to evaluate the flood wave propagation throughout the downstream valleys and obtain the inundation boundaries. The boundaries obtained from HEC-RAS 2D hydrodynamic model were compared to the ones developed by Fernandes et al. (2021) using ANA's Simplified Methodology (SM). Lastly, the delimitation of the Self Rescue Zone and Secondary Security Zone was performed, aiming to help improve Sergipe's dam safety environment.

Characterization of the study area

The Jacarecica River Basin (JRB), Figure 1, is one of the main sub-basins of the Sergipe River Basin (SRB), one of the eight river basins across Sergipe state territory.

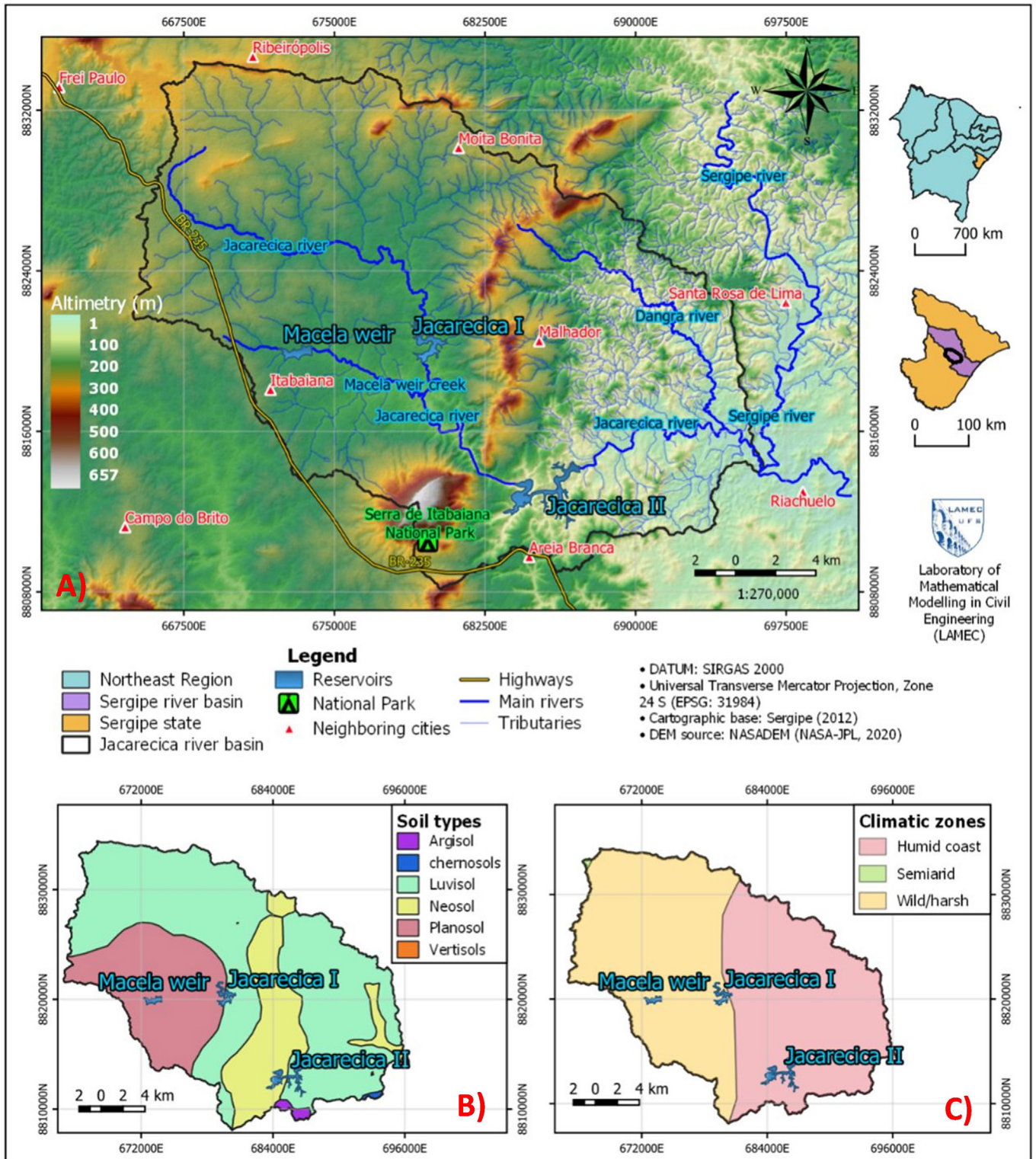
Divided into three climatic zones (wild/harsh, semi-arid and humid coast), the average annual precipitation in the JRB was calculated at 1,063 mm using high-resolution grids (0,25° x 0,25°) of daily precipitation registered throughout Brazil from 1980 to 2013 (Xavier et al., 2016). The rainy season is concentrated between april and august and the dry season between september and march, with the sub-humid dry climate type being predominant (Azevedo & Sousa, 2020).

Despite the existence of the Serra de Itabaiana mountain (peak elevation of 657 m), the terrain across the basin presents characteristics of coastal tablelands, with flattened surface. The valleys are shallow, wide, with flat bottoms and limited by low slopes in most of the JRB. The main river is the Jacarecica, whose waters flow across 67.6 km, receiving contribution mainly from Macela weir creek and Dangra river, until reach its mouth, at the confluence with Sergipe river (Rocha & Almeida, 2020).

According to data obtained from the Sergipe Digital Atlas (Sergipe, 2012), which accounts for the characterization of soil types within the Sergipe state, at a 1:400.000 scale, the predominant soil types in JRB are Luvisol, Planosol and Neosol, wich correlate to the hydrological group D proposed by Sartori et al. (2005).

From Mapbiomas collection 7 (2021), it was perceived that land use in the JRB consists of long strips of exposed soil and pastures, complemented by various agricultural crops, some urban areas and a small portion of native vegetation (Atlantic Forest), mainly close to the Serra de Itabaiana National Park (Sergipe, 2019; Souza Junior et al., 2020).

The irrigated perimeters Jacareica I (JAC-1), located in the village Jacareica, in the rural area of Itabaiana/SE, and Jacareica II (JAC-2), located in the village of Palmeira, in the rural area of Malhador/SE, are formed by obstructions (dams) on the Jacareica River. As they are located on the same river, separated by about 12 km, the JAC-2 dam has a contribution basin that encompasses that of the JAC-1 dam (Figure 2).



Although the JAC-2 contribution basin has a higher drainage density, due, in large part, to the emergence of tributaries to the Jacarecica River at the heights of the Serra de Itabaiana National Park, the JAC-1 contribution basin has a greater tendency to flooding than that of the JAC-1 dam (Sergipe, 2019).

With NASADEM Digital Elevation Model (DEM) (National Aeronautics and Space Administration-Jet Propulsion Laboratory, 2021), the automatic delimitation of the sub-basins in the study region was performed using “r.watershed” and “r.water.outlet” functions of GRASS module within QGIS software. The process consisted in defining the outlets where the lateral boundary conditions (affluent hydrograms) would be entered in the model and delineate the catchment areas to these points, making manual adjustments to accumulate smaller basins eventually generated. The improved altimetry accuracy, vertical error below 10 m, which is a good value to satellite-derived DEMs (Zhang et al., 2019; Uuemaa et al., 2020; Carrera-Hernández, 2021), and complementation of elevation data with the aid of the Advanced Spaceborne Thermal Satellite Emission and Reflection Radiometer (ASTER) Global Digital Elevation Model (GDEM), makes NASADEM product one of the best freely available satellite-derived DEM with global coverage (Courty et al., 2019; Franks et al., 2020; Aziz & Rashwam, 2022).

Land use classification

Eight images (description shown in Table 1) from Planet’s nanosatellites constellation (Planet Team, 2021) were used to perform supervised land use classification with artificial intelligence algorithms (Neural Network, Random Forest and Support Vector Machine) in R software (Abdi, 2020). The advanced spatial and temporal resolution provided by Planet images allow several types of studies, including monitoring dynamic events such as land cover and land use change, ocean spills, flood management and bathymetry (Schumann et al., 2018; Poursanidis et al., 2019; Leach et al., 2019; Nagel et al., 2020; Aragon et al., 2021; Tu et al., 2022; Gonçalves et al., 2023).

Table 1. Planet’s nanosatellite constellation image characteristics.

Attribute	Description
Product	Planet Scope Analytic Ortho Scene
Capture date	October 10, 2020
Spectral resolution	4 bands: 1-blue; 2-green; 3-red; 4-near infrared
Spatial resolution	3 m
Radiometric resolution	Analytic Surface Reflectance (SR): 16-bit
Temporal resolution	Daily
DATUM	WGS 84
Accuracy	RMSE < 10 m
Corrections	Atmospheric and radiometric

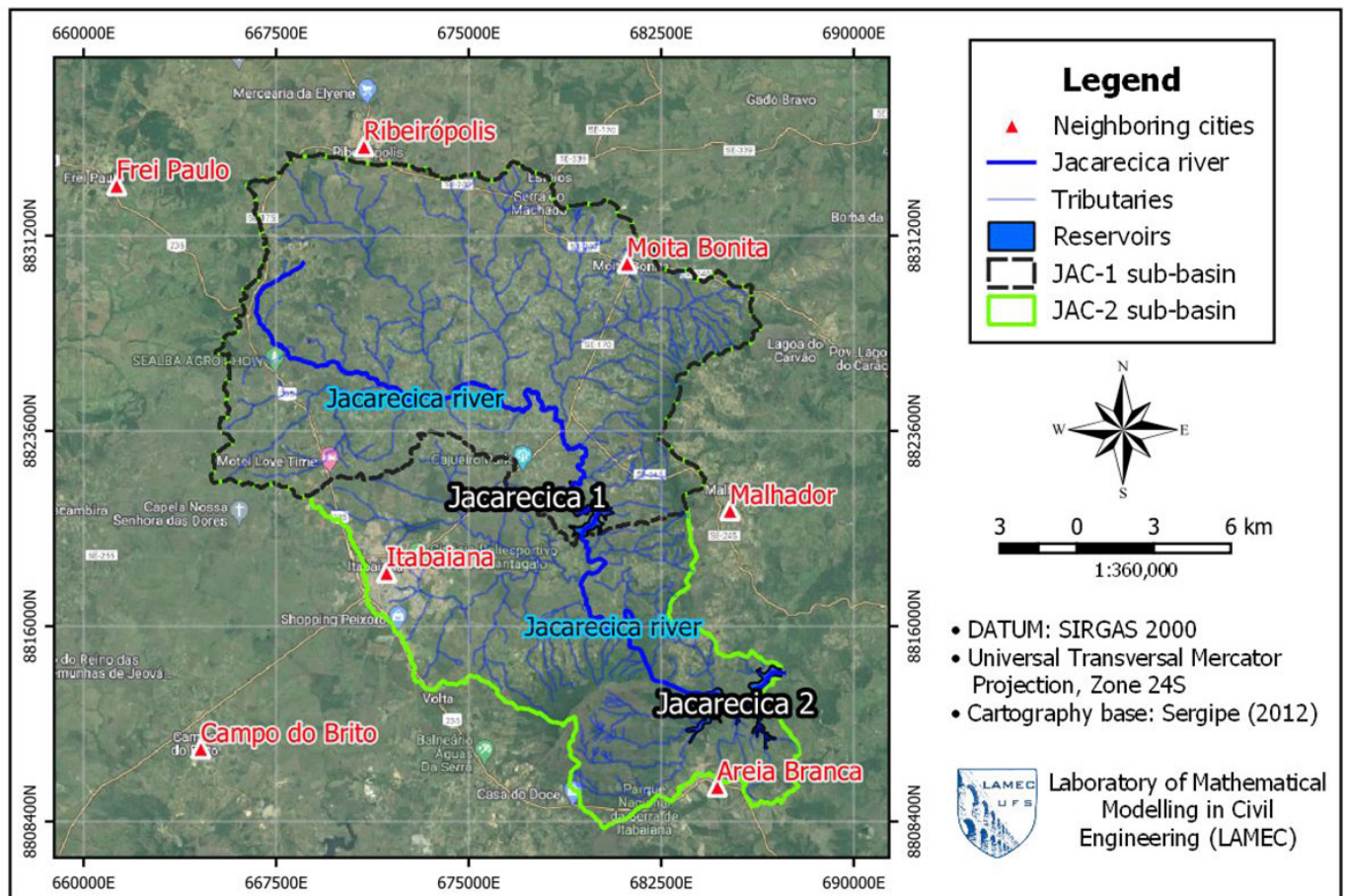


Figure 2. JAC-1 and JAC-2 catchment areas, hydrography and nearby cities.

Supervised classification was chosen because it accomplishes better classification control by the analyst, even though it is subjected to greater subjectivity (Wambugu et al., 2021). Furthermore, non-parametric classifiers (no assumptions made on data statistical distribution) were used because of their performance on multispectral image interpretation (Maxwell et al., 2018; Garg et al., 2022).

Eight land cover categories were considered for classification and, in all eight images obtained of the study area, around 400 points were created for each of them, sampling the pixels that matched the land covers aimed to be classified. After the creation of training layers, the non-parametric classification algorithms (Abdi, 2020) were executed, resulting in codified raster files and confusion matrices, which were then used for performance assessment.

In that regard, the Global Accuracy (GA , Equation 1) and Cohen's Kappa (k , Equation 2) performance indexes were calculated. Global Accuracy measures the ratio between correctly classified observations (principal diagonal in the confusion matrix) and the total observations (total elements in the confusion matrix). Cohen's Kappa index, on the other hand, measures the proportion of classification agreement after casual agreement is disregarded (Lopes et al., 2020; Acharki et al., 2021, Acharki., 2022).

$$GA = \frac{1}{N} \cdot \sum_{i=1}^r X_{ii} \quad (1)$$

$$k = \frac{N \cdot \sum_{i=1}^r X_{ii} - \sum_{i=1}^r (X_{i+} \cdot X_{+i})}{N^2 - \sum_{i=1}^r (X_{i+} \cdot X_{+i})} \quad (2)$$

in which: GA = Global Accuracy ($0 \leq GA \leq 1$); N = confusion matrix total number of observations; r = confusion matrix number of lines (total of categories being classified: eight); X_{ii} = number of observations in line i and column i (elements of principal diagonal); k = Kappa index ($-1 \leq k \leq 1$); X_{i+} = total observations in line i ; and X_{+i} = total observations in column i .

These indexes were automatically calculated in R software after separating the points for 70% training and 30% validation, using cross-validation with 10 subsets (k-folds), standard application of Abdi (2020) classification algorithms. Considering the reference values of k (Table 2), it was possible to assess the agreement of the classification, indicating its performance. Each image was classified three times using the same training layer. The classification that obtained the best AG and k indexes was chosen to compose the region covered by the image.

After the classification, raster files with pixels coded according to Table 3 were obtained. They were then correlated to surface cover reported in Chow (1959) to determine the Manning Coefficient (n), input parameter for roughness in dam break simulations.

The Manning Coefficients considered were the average values reported in Chow (1959). It is noteworthy that these reported values were determined for situations of natural floods, which is very different than a flood induced by a dam break. In these cases, calibration is very difficult, since the inundation reaches places where the natural flood can't. Although uncertainties arise from the choice of Manning Coefficients, i. e. related to the wrong land cover classification and/or variability of Manning's coefficients, the authors considered that using the average values was the best solution for the simulations.

With the results of land use classification, associations between land cover and soil type obtained from Sergipe (2012) were made to determine, in each sub-basin, the average Curve Number (CN), which is one of the parameters used in the Natural Resources Conservation Service (NRCS) CN method for rainfall-runoff transformation. The other parameter is the lag time (T_L), which was determined considering 60% of the concentration time ($T_L = 0.60 \cdot T_c$) of each sub-basin, which was estimated using the USACE empirical equation: $T_c = 0.191 \cdot L^{0.76} \cdot S^{-0.19}$, where T_c is the concentration time (hours), L is the length (km) of the main river and S is the slope (m/m) of the basin.

Hydrological modelling

Using data from Hidroweb platform, daily precipitation time series were obtained in each pluviometric station considered in the study (Table 4). After consistency analysis, gap filling and creation of daily maximum precipitation time series, Mann-Kendal and Spearman non-parametric statistical tests were performed in R software to assess time series' trend and stationarity existence, respectively, procedure recommended in statistical hydrological studies (Barbosa et al., 2021; Isensee et al., 2021; Degraf & Detzel, 2022).

Statistical tests confirmed that the daily maximum time series were stationary and without trend, which allowed the application of the Intensity-Duration-Frequency (IDF) equations, proposed by Aragão et al. (2013), of the cities in the study area (Table 5), to determine reservoirs probabilistic inflow scenarios, as recommended by the Guide for Preparing Emergency Action Plans (Agência Nacional de Águas e Saneamento Básico, 2016).

Table 2. Classification agreement scale based on Kappa Index.

Kappa Index	Level of agreement
$k \leq 0$	Terrible
$0 < k \leq 0.2$	Bad
$0.2 < k \leq 0.4$	Reasonable
$0.4 < k \leq 0.6$	Good
$0.6 < k \leq 0.8$	Very good
$0.8 < k \leq 1.0$	Excellent

Table 3. Association between land use categories, codification used in supervised classification and Manning Coefficient for roughness determination in dam break wave propagation.

Land use categories	code	Manning Coefficient
Agricultural cultivation/caatinga association	1	0.040
arboreal shrubby caatinga	2	0.030
Water	3	0.045
Riparian/seasonal forest	4	0.150
Pasture (fields)	5	0.030
City/township/thorp	6	0.016
Highway (asphalt)	7	0.016
Roadway/exposed soil	8	0.025

To simulate events with different occurrence probabilities, four return periods (T_r) were used: 500, 1,000, 5,000 and 10,000 years. As for the precipitation duration times (t_d), after tests with multiples of the concentration time (t_c), the duration of $t_d = 4.t_c$ was chosen, taking in consideration the recommendation from the Dam Safety Panel (Sergipe, 2015) to adopt this value for critical infrastructure hydraulic/hydrological security assessment.

With pluviometric intensities (i) calculated by the IDF equations, the precipitation depth was obtained for each 5 minutes time interval and then it was distributed: temporally by Huff 50% probability 4th quartile distribution, and spatially by the Areal Reduction Factor (ARF) (Brasil, 2005) and Thiessen Polygon Method. The 4th quartile was defined after trials with different quartiles showed greater direct surface runoff when the precipitation reaches its peak closer to the end of the event, when the watershed soil is already saturated. Furthermore, the ARF was applied because all sub-basins have area greater than 25 km², and so it is recommended to distribute the punctual precipitation calculated from IDF equations throughout the watershed surface area.

With the hyetograms elaborated, the HEC-HMS software was used to perform rainfall-runoff transformation. Concentrated modelling was conducted in each sub-basin, using the precipitation (Huff 4th quartile hyetograms with different T_r associated), infiltration (NRCS-CN Method) and transformation (NRCS's unit hydrogram) modules. The NRCS infiltration and transformation models were used because of their simplicity, large utilization and small quantity of parameters needed, which is adequate for application in non-monitored watersheds (Moglen et al., 2022). Thus, hydrograms were obtained in each sub-basin outlet, representing the lateral flow in every confluence with the Jacarecica river. It is noteworthy to mention that there are no fluviometric monitoring in the study area, which made it difficult to calibrate the hydrological model used to determine the hydrograms. This challenge in calibrating and validating models due to data scarcity is also reported in some studies in arid and semi-arid basins (Alizadeh & Yazdi, 2023) and in Northeast Brazil watersheds (Koch et al., 2020).

Dam-break simulations

According to Agência Nacional de Águas e Saneamento Básico (2016), in dam-break studies, different failure scenarios should be considered, involving the variation of input data, to mitigate the uncertainties they bring to the process. Using HEC-RAS 2D, version 6.0 (United States Army Corps of Engineers, 2021), hypothetical dam break studies were conducted in Jacarecica I (JAC-1) and Jacarecica II (JAC-2) dams considering variations in the following input data: (i) reservoirs initial storage; (ii) water elevations that trigger breach formation; and (iii) affluent hydrograms correspondent to different hydrological events' return periods.

Breach formation parameters

For JAC-1 dam (concrete gravity), a breach caused by a monolithic failure and developed in the spillway was designed, with the following dimensions: B_b (breach base width) of 30.0 m, H_b (breach height) of 10.0 m, Z (sidewall slope horizontal component for the assumed breach trapezoidal section) of 0, t_f (breach time formation) of 0.20 h and sinusoidal law of breach progression in time. These parameters were defined according to values reported in the literature (Campos et al., 2020; Zhong et al., 2021; United States Army Corps of Engineers, 2021; Mei et al., 2023) and also the local analysis of the studied structures dimensions.

Regarding JAC-2 dam (embankment dam, pipping failure), three breach formation empiric models often applied in dam breach modelling were utilized (Table 6). Already built in HEC-RAS 6.0, the models calculate breach average width (B_{av}), trapezoidal breach side slope horizontal component (Z) and formation time (t_f) given input parameters such as reservoir maximum capacity and height of water above breach bottom. For JAC-2 dam, these parameters are equal to 26.23 hm³ and 10.0 m (considered breach height). Thus, breach dimensions and formation time from these 3 models were obtained and the results from the Froehlich (2008) model (study more recent and that used more historical data to adjust the empirical equations) were utilized.

Table 4. Pluviometric stations utilized for hyetogram design in each sub-basin.

Code	Station name	Operator	Data period	Latitude / Longitude	Altitude (m)
01037008	Campo do Brito	SUDENE	1593 – 2000	-10.75 / -37.50	180
01037014	Frei Paulo	DNOCS	1913 – 1984	-10.55 / -37.53	272
01037030	Malhador	SUDENE	1963 – 1984	-10.67 / -37.30	224
01037044	Ribeirópolis	DNOS	1963 – 1999	-10.53 / -37.43	350

Table 5. IDF equations parameters.

Municipality	k	a	B	c
Malhador	960.7	0.164	10.52	0.753
Ribeirópolis	1,080.5	0.061	10.52	0.753
Campo do Brito	868.3	0.204	10.52	0.753
Frei Paulo	795.3	0.135	10.52	0.753
Nossa Senhora das Dores	838.7	0.161	10.52	0.753
Siriri	1,004.3	0.161	10.52	0.753
Santa Rosa de Lima	1,022.9	0.088	10.52	0.753
Riachuelo	944.2	0.110	10.52	0.753

Table 6. JAC-2 dam breach dimensions and formation times obtained from empirical models.

Equation	B_{ave} (m)	t_f (h)	H_B (m)	Z
Von Thun & Gillette (1990)	79.9	2.0	10.0	0.40
Froehlich (1995)	92.5	2.7	10.0	1.40
Froehlich (2008)	91.0	2.9	10.0	1.00

Table 7. Water surface elevations (m) related to initial storage percentage.

reservoir	storage percentage (%)		
	50	75	100
Jacarecica I (JAC-1)	145.30	146.80	148.07
Jacarecica II (JAC-2)	63.11	67.22	70.39

Table 8. Scenarios for trigger failure at different elevations.

Reservoir	TFA-1 (m)	TFA-2 (m)*
Jacarecica I	149.74	153.22
Jacarecica II	72.56	77.04

*Considering additional 15 cm of water elevation above dam crest to simulate overtopping failure, as recommended by Agência Nacional de Águas e Saneamento Básico (2016).

Initial storage

Initial reservoir storages of 50%, 75% and 100% maximum capacity (4.05 hm³ for JAC-1 and 26.23 hm³ for JAC-2) were considered to compose the varying scenarios. Using the reservoirs' elevation-area-volume curves (Sergipe, 2018), water surface elevation correspondent to the storages were calculated, as presented in Table 7.

Water surface elevation for failure trigger

Aiming to simulate scenarios where the spillways (open air, surface flow, no gates) operate, two water surface elevations above their crest were considered as failure trigger (Trigger Failure At – TFA): the first elevation (TFA-1) was considered at one third of the spillway height (difference between the dams crests and the spillways sills); and the second one (TFA-2) located at the dams' crest plus a lag of 15 cm. These elevations, shown in Table 8, were chosen to simulate failures due to internal erosion/monolithic fail (TFA-1) and overtopping (TFA-2).

Affluent hydrograms

Reservoirs' affluent flows were obtained through rain-runoff transformation using NRCS-CN method on HEC-HMS and also through flood propagation (Shallow Water Equations) along Jacarecica river on HEC-RAS.

Each delimited sub-basin was loaded in HEC-HMS separately, as concentrated models. The input data were the basins' average Curve Number (CN_{AVE}) and Lag Time (T_L), and the designed hyetograms, spatially (ARF and Thiessen coefficients) and temporally (50% probability, 4th quartile Huff distribution) distributed.

Return periods of 100, 500, 5,000 and 10,000 years were utilized to generate different probabilistic hydrograms for dam break simulations.

Hence, the flow affluent to the JAC-1 reservoir represented the outlet flow from its catchment area. For JAC-2 reservoir, the affluent flow was obtained from the flood propagation along Jacarecica river, accounting for JAC-1 spillway outlet and/or dam break flow and the lateral contributions at confluences.

Most probable and extreme failure scenarios

Following recommendations from reference literature such as Federal Emergency Management Agency (2013) and Agência Nacional de Águas e Saneamento Básico (2016), the most probable and extreme failure scenarios were considered in this study. The first one considers the rupture occurring during dam's usual operating conditions and affluence inflows. The second one involves worsening in hydrometeorological conditions, simulating the failure happening at extreme events. In other words, ruptures on sunny day (in which the reservoir is at normal full pool elevation and normal flow at downstream talwegs is prevailing) and rainy day (hydraulic structures at full capacity and flood flow conditions at downstream talwegs causing natural inundation at higher elevations) were also accounted for.

Considering that the maximum capacity at normal operation corresponds to the spillway sill elevation, that overtopping happens when the reservoirs' water surface reaches dam crest elevation plus a gap of 15 cm and that breach parameters were chosen as previously described, the input data to simulate the most probable rupture (MP) and extreme rupture (ER) scenarios are shown in Table 9.

For the MP, initial storages were defined below maximum capacity, to simulate usual operating conditions. As for the ER, the initial storage represents the reservoirs' maximum capacity. With these scenarios and the NASADEM digital elevation model, the spatialized Manning Coefficients and the full-momentum Saint-Venant equations (Shallow Water Equations), the dam break simulations were performed in HEC-RAS 2D.

JAC-1 reservoir (wide and short pool) was modeled as storage area (level pool routing) and JAC-2 reservoir (long and narrow pool) was modeled as 2D Flow Area (full unsteady flow routing).

Table 9. Most probable and extreme scenarios proposed for the study.

Scenarios	TR (years)	Init. Stor. (%)	Jacarecica I					Jacarecica II				
			TFA (m)	B (m)	H (m)	Z	Tf (h)	TFA (m)	B (m)	H (m)	Z	Tf (h)
<i>Most probable failure</i>												
Sunny day	100	50	149.74	30	10	0	0.20	72.56	91	10	1.0	2.9
Rainy day	5,000	75	153.22					77.04				
<i>Extreme failure</i>												
Sunny day	500	100	149.74	36	12	0	0.17	72.56	109.2	12	1.2	2.4
Rainy day	10,000	100	153.22					77.04				

TR: Hydrometeorological event's return period; **TFA:** Trigger Failure At (water elevation that triggers breach); **B:** Width of the breach; **H:** Height of the breach; **Z:** horizontal component of breach's trapezoidal section lateral slope; **T_f:** Formation time of the breach.

The computational mesh resolution was set to 50 x 50 m in all modeled domain, but refinement regions with smaller mesh resolutions (10 x 10m around Jacarecica II reservoir and Riachuelo city, and 5 x 5m along water courses) and break lines were considered along rivers' center lines, confluences, before and after structures such as dams and bridges. Boundary conditions were lateral flows, initial storage, breach parameters and normal depth. The computational time step was set to vary according to Courant number, one of the new functionalities of HEC-RAS 6.0 (United States Army Corps of Engineers, 2021).

Besides the inundation boundaries elaboration, simulation results (maximum flow, depth and velocities) were extracted in determined cross sections along JAC-2 downstream floodplain to compare HEC-RAS (hydrodynamic model) results to the ANA's Simplified Methodology (Fernandes et al., 2021), which is explained in the last topic of this section.

ANA's simplified methodology (SM)

The application of empirical models in dam break studies becomes an alternative when there isn't sufficient input data for more robust models, which is a reality in the Brazilian context (Pereira et al., 2017; Kanani-Sadat et al., 2019; Fernandes et al., 2021; Mudashiru et al., 2021). An example of empirical modeling is the Simplified Methodology (SM) adopted by the National Water and Sanitation Agency (Agência Nacional de Águas e Saneamento Básico, 2017) to classify dams in terms of the associated potential damage (DPA). This model was initially developed by the United States Army Corps of Engineers (USACE), which performed a statistical analysis on a database of 145 real failures to establish empirical expressions that determine the limits of the area compromised by a possible dam failure (Agência Nacional de Águas e Saneamento Básico, 2017).

Developed for APD classification purposes, the SM uses available information on the location of dams, water courses and altimetry to, using empirical equations, determine the extent of the flooded area, the breach peak flow and the propagation of this flow along the downstream channel. For detailed information on this matter, refer to Agência Nacional de Águas e Saneamento Básico (2017).

A recent development for this methodology was presented by Rolo et al. (2023). In their work, a python implementation for the ANA's original methodology is proposed as an alternative to be applied in less time and with less user interaction, which can

be quite useful for government agencies and dam entrepreneurs in a low budget.

Therefore, this work compares the results obtained from the application of the hydrodynamic model (HEC-RAS) and the SM to the Jacarecica II downstream valley (Fernandes et al., 2021). The inundation boundary areas (considering the same extension modelled by the SM) and maximum flow, depth and velocities at the 21 stations located by the SM were compared through the percentual difference (Equation 3), considering HEC-RAS (HR) results as the reference values.

$$Difference(\%) = \frac{variable_{SM} - variable_{HR}}{variable_{HR}} \quad (3)$$

Inundation mapping and risk zoning

For the sunny day most probable rupture (SDMP) and sunny day extreme rupture (SDER) scenarios, the inundation boundary was plotted, showing the flood waves' spatial scope. Also, for the same scenarios, the delimitation of the Self Rescue Zone (SRZ) and the Secondary Save Zone (SSZ), important hazard zones in Emergency Acting Plans (EAP), was performed.

According to Agência Nacional de Águas e Saneamento Básico (2016), the SRZ is defined as the farthest of two distances: 10 km ahead the dam axis or the distance travelled by the flood wave in a 30-minute interval. As for the SSZ, it can be delimited considering the distance travelled by the flood wave in a 120-minute interval. These hazard zones were obtained along JAC-2 downstream valley, where villages, isolated households, agricultural lands and transportation infrastructure were identified.

RESULTS AND DISCUSSION

Sub-basin delimitation and land use classification

The sub-basin automatic delimitation result is shown in Figure 3 whereas some planialtimetric and morphometric parameters usually calculated to characterize catchment areas are displayed in Table 10.

Adding up the area of sub-basins Jac1, Ac.Mac, Incr. e Dang. (Table 10), which comprehend the Jacarecica river sub-basin (JSB), the outcome is 500.24 km², result that is 7,05 km² smaller than the one obtained by Rocha & Almeida (2020).

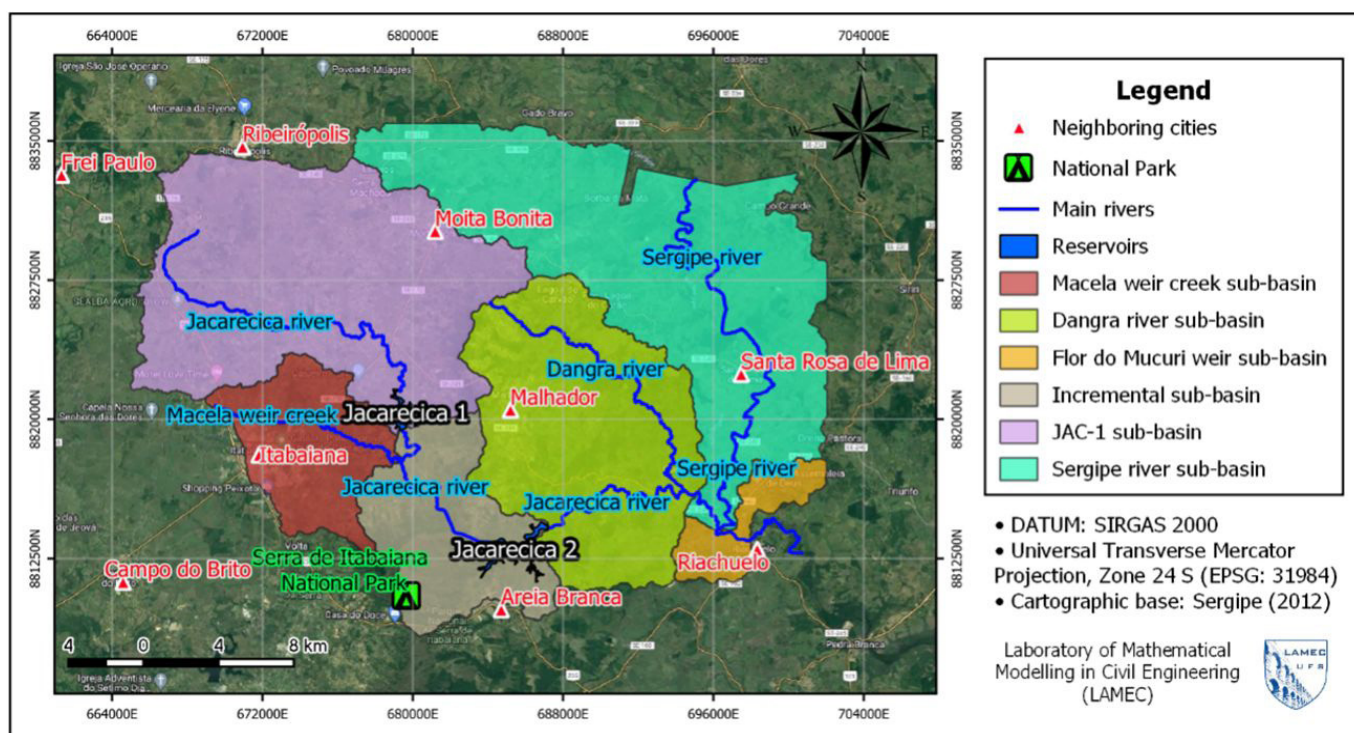


Figure 3. Automatically delimited sub-basins, its main rivers and cities within study area.

Table 10. sub-basins' planialtimetric and morphometric parameters.

Parameters	Jac1	Ac.Mac.	Incr.	Dang.	Serg.	F.Muc.
Area (km ²) – \mathcal{A}	211.94	59.52	75.29	153.49	225.98	22.37
Perimeter (km) – P	104.78	52.49	57.89	76.86	127.96	34.65
Axial length (km) – L_A	19.12	9.03	10.32	14.68	18.56	10.14
Drainage length (km) – D_L	299.14	76.39	146.78	411.88	520.14	40.35
Maximum altitude (m) – H_{MAX}	485	582	657	483	383	142
Main channel length (km) – L_{MC}	32.17	13.45	18.33	24.32	37.37	7.67
Main channel altitude range – ΔH_{MC}	91	80	79	267	41	34
Main channel slope (m/m) – S_{MC}	2.83	5.95	4.31	10.98	1.10	4.44
Drainage density (km ⁻¹) – D_D	1.41	1.28	1.95	2.68	2.30	1.80
Compacity Coefficient (dim.) – k_C	2.02	1.91	1.87	1.74	2.38	2.05
Form Factor (dim.) – F_F	0.58	0.73	0.71	0.71	0.66	0.22
Concentration time (min) – T_C	488.64	218.78	294.27	305.33	655.63	150.83

Jac1: catchment area of Jacarecica I dam; **Ac.Mac.**: Açude Macela stream sub-basin; **Incr.**: Incremental sub-basin between JAC-1 and JAC-2 dams, disregarding the Açude Macela stream sub-basin; **Dang.**: Dangra river sub-basin; **Serg.**: Part of Sergipe river basin within study area; **F. Muc.**: Flor do Mucuri stream sub-basin; **dim.** = dimensionless; $S_{MC} = \Delta H_{MC} / L_{MC}$; $D_D = D_L / A$; $k_C = 0.28 \cdot P / \sqrt{A}$; $F_F = A / L_A^2$; $T_C = 11.46 \cdot L_{MC}^{0.76} / S_{MC}^{0.19}$.

Although this difference exists and that the Sergipe river basin was considered in a small portion of its total size, the delineation process performed in the study revealed sub-basins with reasonable sizes for the dam break study, which requires specific and local information for adequate performance (Tschiedel et al., 2020; Mohanty et al., 2020).

According to Table 10, the Dangra river sub-basin is the most susceptible to flooding and rapid flows, considering the greatest S_{MC} and D_D , and the high F_F and D_L . This conclusion can be confirmed observing that the same sub-basin has the smallest k_C (the closer to 1, the more circular is the sub-basin, and thus more susceptible to flooding) and the quotient between T_C and D_L , indicating that the water precipitated takes small time to travel

through the basin and reach the outlet. Considering the obtained sub-basins, the land use classification result is shown in Figure 4 and Table 11.

From Figure 4, it can be noticed that a large part of the classified area is covered by pastures, arboreal shrubby Caatinga and seasonal forest, which is a characteristic of the rural region in which the study area is located (Rocha & Almeida, 2020). Other uses are more localized, such as agricultural crops nearby irrigated perimeters or urban areas, being the municipality of Itabaiana the largest one.

Still analyzing the Figure 4, it is possible to identify a small empty part (non-classified) in the Dangra river sub-basin and a cropped portion in the upper part of the Sergipe river sub-basin.

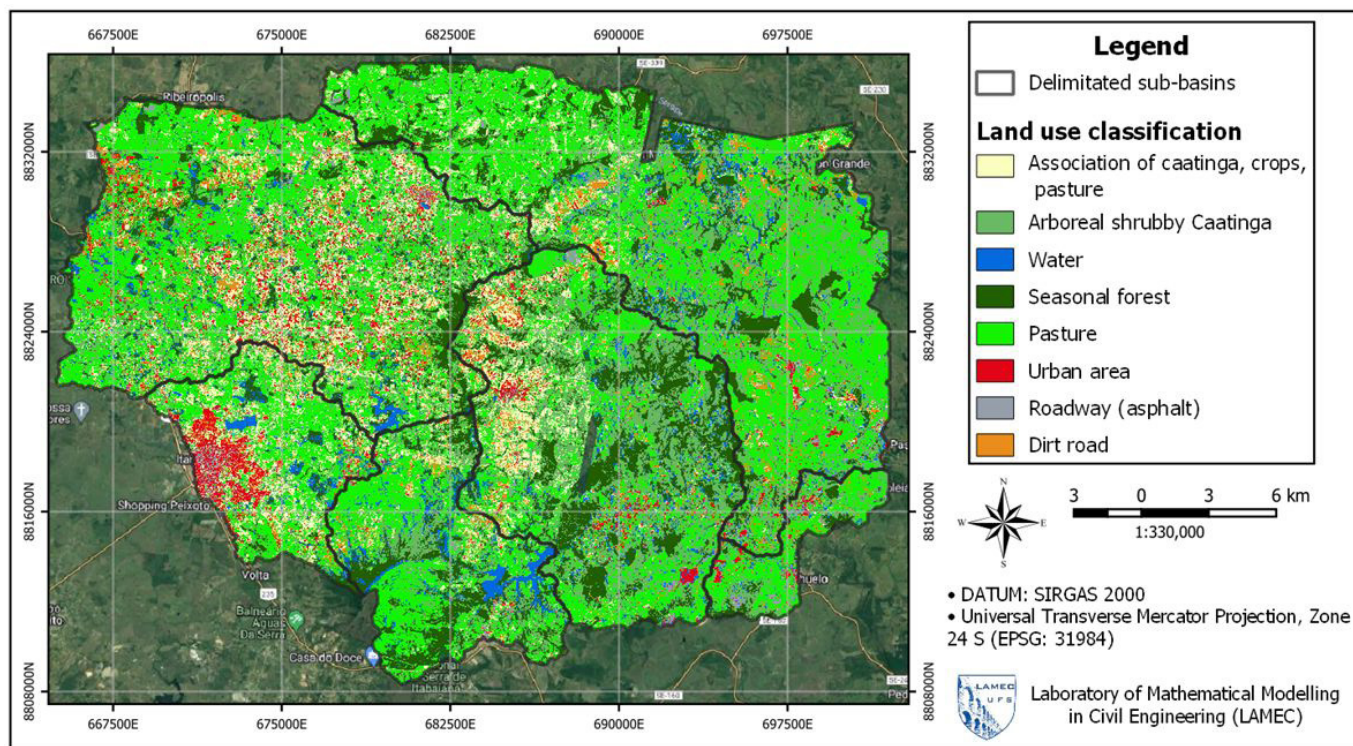


Figure 4. Study area land use classification map.

Table 11. Supervised classification results using machine learning algorithms.

Image	RF		SVM		NN	
	GA	k	GA	k	GA	k
1	0.811	0.780	0.838	0.812	0.387	0.268
2	0.847	0.820	0.865	0.842	0.446	0.345
3	0.816	0.783	0.838	0.810	0.341	0.167
4	0.781	0.744	0.774	0.736	0.382	0.257
5	0.760	0.725	0.771	0.737	0.440	0.359
6	0.820	0.788	0.840	0.812	0.401	0.267
7	0.863	0.842	0.876	0.857	0.396	0.293
8	0.818	0.784	0.834	0.802	0.509	0.403
Mean	0.815	0.783	0.830	0.801	0.413	0.295

RF: Random Forest; SVM: Support Vector Machine; NN: Neural Network; GA: Global Accuracy; k: Cohen's Kappa Index.

These failures are due to inadequate overlapping of the satellite's paths when images were captured by its sensors. Although these flaws have been revealed, they are insignificant considering the classification capacity that Planet images allow: with a spatial resolution of 3.0 m, the classification of land use is much more detailed when compared to the same product available in the Mapbiomas project, collection 7 (Figure 5), based on Landsat satellite images (Souza Junior et al., 2020).

With the result shown in Figure 4, the classified land use categories were associated to Manning Coefficients (Table 3) to obtain the 3 m spatial resolution Manning coefficient shapefile layer, parameter needed to characterize terrain roughness in dam-break simulations. As mentioned, the association was made considering coefficients reported in literature (Chow, 1959), which were defined based on land cover identified with satellite image investigation of the study area.

Rainfall-streamflow modelling

The non-parametric statistical tests applied, revealed that annual maximum daily precipitation time series are stationary and without trend, considering 5% significance interval. Thus, the IDF equations proposed by Aragão et al. (2013), developed under non-stationarity and no trend premises, could be properly used (Ouarda et al., 2019). Using the methodology described previously, the precipitation was spatially and temporally discretized in all sub-basins, resulting in hyetograms with peak precipitation depths presented in Table 12.

The hyetograms, together with the CN_{AVE} and lag time, were then used in the rain-runoff transformation on HEC-HMS (NRCS Unit Hydrogram Method) to obtain the outlet hydrogram in each sub-basin. Due to the lack of fluviometric gauges in the studied sub-basins, it wasn't possible to properly calibrate/validate the hydrologic model.

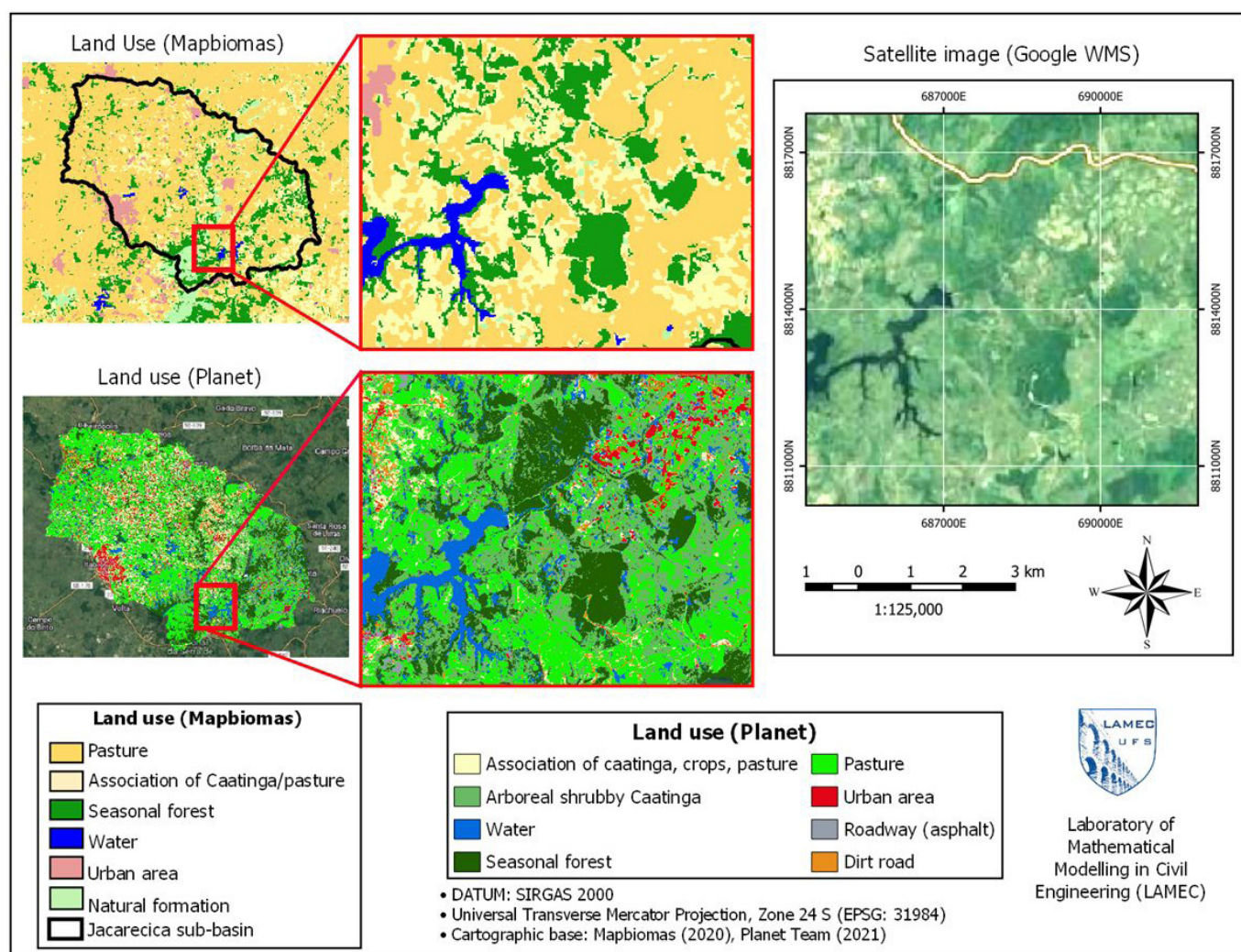


Figure 5. Comparison between land use maps obtained from Planet images and Mapbiomas Collection 7.

Table 12. Maximum precipitation depth in 5 minutes interval in each sub-basin, considering Huff 50% 4th quartile temporal distribution and Thiessen and ARF coefficients for spatial distribution.

Sub-basin	T_d (hours)	Return Period (years)			
		100	500	5,000	10,000
Jac1	32.4	1.14	1.37	1.81	1.98
Ac.Mac.	14.4	2.69	3.58	5.41	6.13
Incr.	19.6	2.08	2.70	3.94	4.42
Dang.	20.4	1.93	2.50	3.60	4.02
Serg.	43.6	0.92	1.12	1.42	1.60
F. Muc.	10.0	2.68	3.19	4.11	4.44

T_d = Precipitation duration time, calculated as four times the concentration time in each sub-basin (Sergipe, 2015).

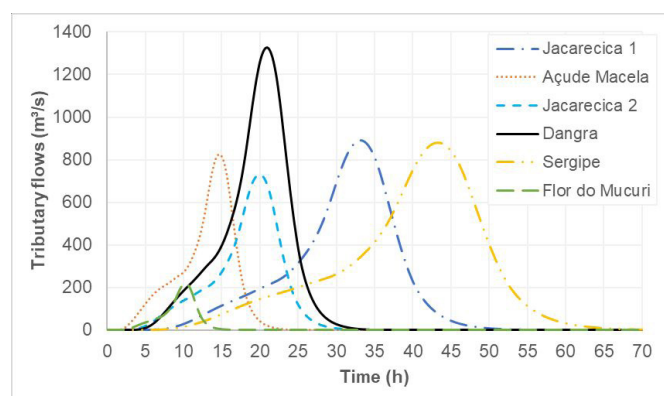
However, considering the high spatial resolution of the Planet images (3 m), used for land cover classification, which allowed the CN calculation; and the sub-basin delimitation and planialtimetric characterization performed with the NASADEM, best global DEM freely available, the input parameters (CN_{AVE} and lag time) obtained for hydrological modelling were considered adequate for the purpose of the study.

The peak discharges calculated for each sub-basin, considering the different return periods, are demonstrated in Table 13 and the resulting hydrogram in each sub-basin is shown in Figure 6.

It can be noted that the rain-runoff transformation in Dangra river sub-basin resulted in hydrograms with higher maximum flow for all return periods, which can be explained by its high susceptibility to flood. The same analysis applies to the Sergipe

Table 13. Peak discharge ($\text{m}^3\cdot\text{s}^{-1}$) resulting from rain-runoff modelling of each sub-basin.

Sub-basin	Return Period (years)			
	100	500	5,000	10,000
Jac1	444.18	567.39	801.82	888.81
Ac.Mac.	339.27	467.29	726.52	827.67
Incr.	295.18	412.74	644.23	732.32
Dang.	509.43	727.98	1,161.70	1,326.67
Serg.	463.92	589.61	796.68	908.94
F. Muc.	117.57	147.10	199.43	217.89


Figure 6. Affluent hydrograms in all sub-basins for TR of 10,000 years.

river sub-basin, which has similar morphometric parameters and demonstrated the second highest peak discharge.

Considering the return periods used in the study, it was expected that considerable peak flows would result from the rain-flow transformation. In the study carried out by Sergipe (2019), a decamillennial inflow of $2,566.3 \text{ m}^3/\text{s}$ was estimated for the Jacarecica I dam (Jac1 contribution basin). However, as the methodology for its determination was different (concentration time obtained by Kirpich equation, construction of hyetograms by alternating blocks, longer rain duration, disregard of the DEM in the rainfall-runoff modeling with HEC-HMS and CN parameter determined based on land use layer present in the Sergipe Digital Atlas), the result mentioned on the referred study seems to be overestimated. In the report presented by the Dam Safety Panel (Sergipe, 2015), a peak decamillennial flow of $574.85 \text{ m}^3/\text{s}$ was obtained for the same sub-basin, a value much lower than that obtained by Sergipe (2019). Comparing these studies to the results obtained in this research, with the available data and considerations made, it is believed that the present results are adequate.

Dam-break inundation mapping

Using the dam-break scenarios proposed in Table 9, the simulations were performed in HEC-RAS 6.0 2D model, considering the full dynamic Shallow Water Equations. It was observed that both dams fail under the sunny day most probable scenario (SDMP), whereas for the rainy day (RDMP) it didn't happen, even though more intense hydrological events were simulated. The reason for

that is the designed failure mode: monolithic failure/internal erosion for sunny day and overtopping for rainy day. This confirms the conclusion made by the Dam Safety Panel (Sergipe, 2015) that the dams are secure to overtopping.

Although this fact, the inundated area in the rainy day most probable scenario (14.34 km^2) was slightly greater than the one resulting from the sunny day most probable scenario (13.65 km^2), when both dams breach. Even though breaches only happen in sunny day scenario, the intense hydrometeorological condition simulated in rainy day scenario causes the release of significant flows from hydraulic structures, contributing to greater floodplain occupation (Figure 7).

It can be noted that in both scenarios, the flooded area comprises agricultural land, pasture, some riparian vegetation and residential areas, specially at Riachuelo city, where the dam-break wave takes from 8 to 9 hours to reach its peak (sunny day scenario) and depths of 10 m and velocities of $3,7 \text{ m}^3\cdot\text{s}^{-1}$ were observed (rainy day scenario).

As for the extreme rupture scenarios, the pattern remained: the dams fail in sunny day scenario (erosion/monolithic failure) but not in rainy day (overtopping failure). The breaches predicted in the first case guaranteed rupture and the flood wave propagation throughout downstream valleys. In the second case, even though both dams start the simulations with initial storage at 100% of capacity and receiving affluent flows greater than the ones defined for the most probable scenarios, the dams' spillways were able to discharge the accumulated volumes without crest overcome. This fact proves again that the dams are safe to overtopping (Sergipe, 2015), even if decamillennial hydrological events are simulated.

Another important analysis in dam break studies is the delimitation of the Self Rescue Zone (SRZ) and the Secondary Save Zone (SSZ). As recommended by Agência Nacional de Águas e Saneamento Básico (2016), the risk zoning was made considering the traveled distance within 30 minutes of dam breach for SRZ and 120 minutes for SSZ. Analyzing the Figure 8 details, it can be noted the existence of houses (yellow circles), local roads, agricultural land and pasture inside the SRZ and SSZ.

This result enforces the immediate need to develop Emergency Acting Plans (EAP) for both dams, especially JAC-2, since there are villages, agricultural lands, an industry, transportation infrastructure and, at about 18 km from the dam, the city of Riachuelo in its downstream valley.

Similarly to the most probable rupture scenario, the inundation simulated in extreme scenarios extended to a vast area: 14.55 km^2 for sunny day extreme rupture (SDER) and 15.01 km^2 for rainy day extreme rupture (RDER). Not only the inundated area,

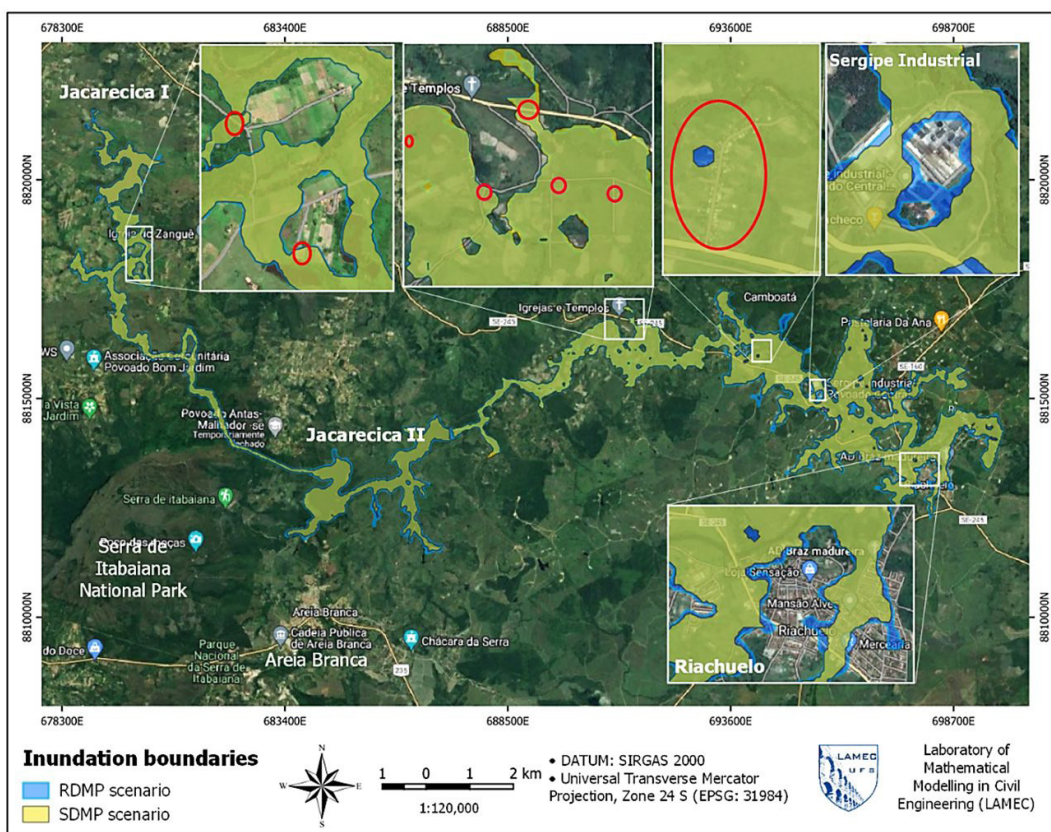


Figure 7. Inundation boundaries resulting from the most probable sunny and rainy-day scenarios.

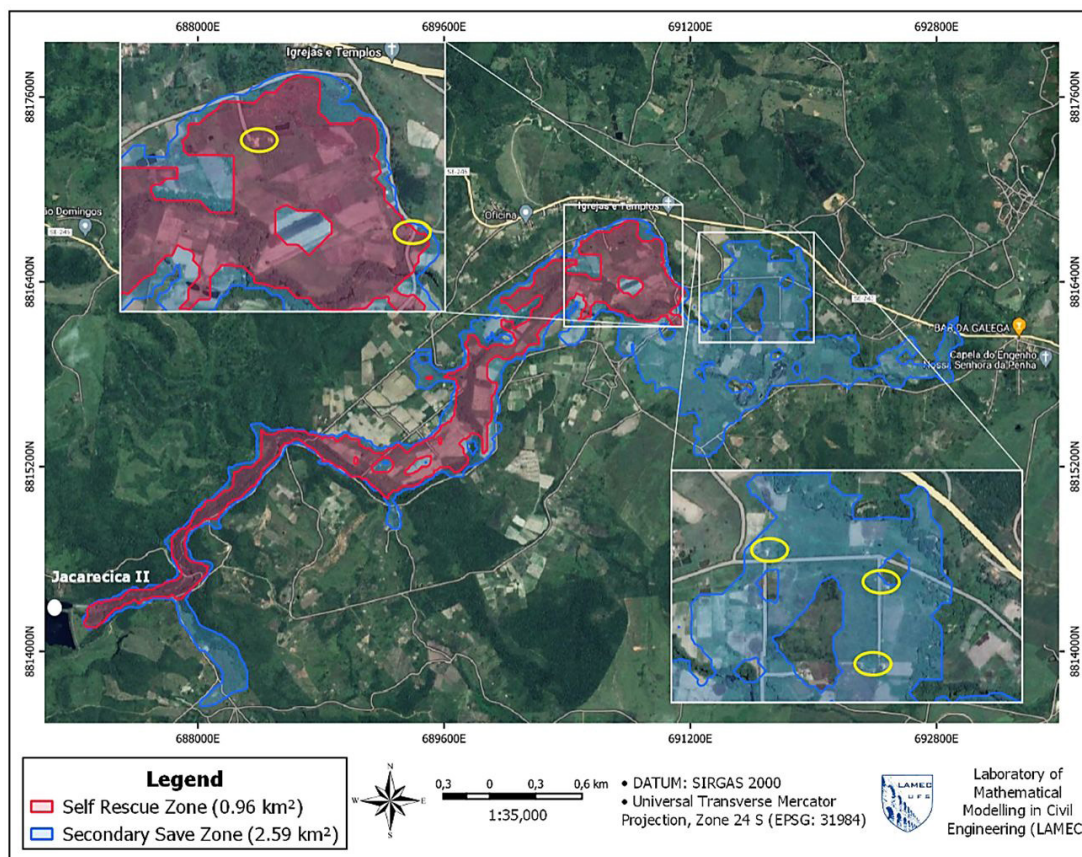


Figure 8. SRZ and SSZ delimitation for sunny day most probable rupture scenario.

but the spatial disposition of the boundaries was also similar to the ones obtained for most probable scenarios (Figure 7): almost the same areas were impacted, but with changes in the magnitude of the boundaries. For example, the maximum depth and velocity at Riachuelo were registered at 10 m and 4,5 m.s⁻¹, respectively, and the dam break wave takes minimal 6 to 8 hours to reach the city. Finally, the risk zoning for SDER is presented in Figure 9, that shows a wider area at risk, as expected.

Although there are dam failure studies reported in the literature, the particular characteristics of the dams and the downstream topography lead to results that are mostly linked to the domain where the simulations occurred. Thus, comparing simulation results of dam break studies requires precaution.

For example, Hosseinzadeh-Tabrizi et al. (2022) simulated the propagation of the Sattarkhan dam failure using 2D HEC-RAS model. The study area has similar occupation (industrial, residential, agricultural areas) and the dam extension and height are in the same order of magnitude of the Jacarecica II dam. Two scenarios were simulated, resulting in maximum depths and velocities of the same proportion obtained in the present work, around 9 m and 5 m/s, respectively.

Haltas et al. (2016) simulated the Ürkmez Dam failure, a structure of 46 m height and with a 7.6×10^6 m³ capacity. The breach was modeled after application of Froehlich (2008) empirical model, resulting in a trapezoidal-shaped breach with dimensions similar to the ones obtained using the same empirical model in Jacarecica II dam. It was used FLO2D model to run the simulation, using DEM, land cover and soil type maps supplied by public agencies. The computational domain covered a great proportion of urban area and the results of depth and velocity were similar to the ones calculated over the Riachuelo city.

It is noteworthy that the results demonstrated rely on the quality of the input data and the capabilities of the numerical model used. These and other uncertainties are common when using dam break models (Tschiedel & Paiva, 2018; Pinheiro et al., 2019; Hu et al., 2020).

In order to assess the uncertainties, a sensitivity analysis was performed. It consisted in the calculation of the coefficient of variation (CV) for hydrodynamic results (velocity, depth and flow rate) at 8 observation points throughout the downstream floodplains as the input data (breach geometry, initial reservoirs storages and water level that triggered the failure - TFA) varied.

The sensitivity analysis concluded that the flow rate and the depth are more sensible to the variation of the TFA (maximum CV of 0.35 and 0.11, respectively). The change in breach configuration has provoked a greater CV for the velocity results (maximum CV of 0.20). Lastly, the variable initial reservoir storage hasn't caused significant change in CV.

Event though there were some variation in the hydrodynamic results with changing scenarios, the simulations performed was considered to be adequate, given the quality and availability of input data.

The remotely sensed DEM used for the simulations brings uncertainties to the results and, as mentioned by Azizian & Brocca (2020), can lead to considerable errors, especially in flood's inundated extents and water level results. McClean et al. (2020) also reported that the impact of flooding simulations

using Global Digital Elevation Models (GDEM) is overestimated, compared to the obtained with airborne LIDAR-derived DEM (considered gold-standard for DEM data collection). In contrast of these considerations, Fleischmann et al. (2019) reported that a locally derived DEM did not lead to significant improvements in relation to a global DEM for flood extent simulations.

Nevertheless, considering the lack of more accurate data, i.e. LiDAR-derived DEM, it represents the best topographic information to simulate the flood boundary due to the dams' failure.

Comparison to ANA's Simplified Methodology (SM)

The ANA's SM, designed for dam's associated potential damage classification, was applied to the Jacarecica II dam by Fernandes et al. (2021). In this study, the inundation boundary and the maximum velocity, depth and flow at 21 cross sections were obtained. Aiming to compare the results obtained in this work, which used the HEC-RAS (HR) hydrodynamic model, with the SM, the HR results of the same variables were extracted at the same locations and the percentual difference (% diff) was calculated considering HR results as reference.

Comparing the spatial coverage of the inundation boundaries obtained by the SM and by the sunny day most probable (SDMP) and extreme (SDER) rupture scenarios, it can be noted how the SM overestimates the flooding (Figure 10). In addition to the difference between the contours observed in Figure 10, the total flooded areas (SM: 7.61 km²; SDMP: 5.06 km²; SDER: 5.39 km²) confirm this conclusion. It is noteworthy to mention that this overestimation is due to the premises adopted by SM (Agência Nacional de Águas e Saneamento Básico, 2017), which are not considered in HEC-RAS hydrodynamic model.

The percentual differences between maximum velocities and depths were calculated for HR and SM outputs at the 21 cross sections used by the SM to elaborate the inundation boundary. For the maximum flow comparison, the percentual difference was one order of magnitude higher than the differences obtained for velocity and depth. The overestimated maximum flow resulting from the SM is the reason for this to happen.

Observing Figure 11 and Figure 12, it is possible to conclude that the SM tends to provide greater depths and lower velocities (especially in sections further away from the dams) compared to the HR responses in both scenarios (SDMP and SDER).

To obtain the velocity and depth, the SM uses the flows calculated in each section (as a function of the overestimated rupture flow in the dam axis) and, with the NASADEM DEM, determines the flow area in the section. With the Manning-Strickler equation, the flow heights and velocities in each section are obtained. Therefore, the resulting depths tend to be greater and the velocities, thus, reduced, when compared to the HR responses, that are obtained using the same DEM, but with full momentum hydrodynamic equations.

As for the values of the maximum flows obtained with the ruptures, it is prudent to emphasize that they depend on the breach formed. SM considers total dam body failure, an extreme case of failure that occurs more frequently in concrete arch dams, for instance. The HR model, otherwise, considers user-entered breach parameters or calculates them using dam parameters in empirical equations, which results in smaller breaches and, therefore, lower peak flows.

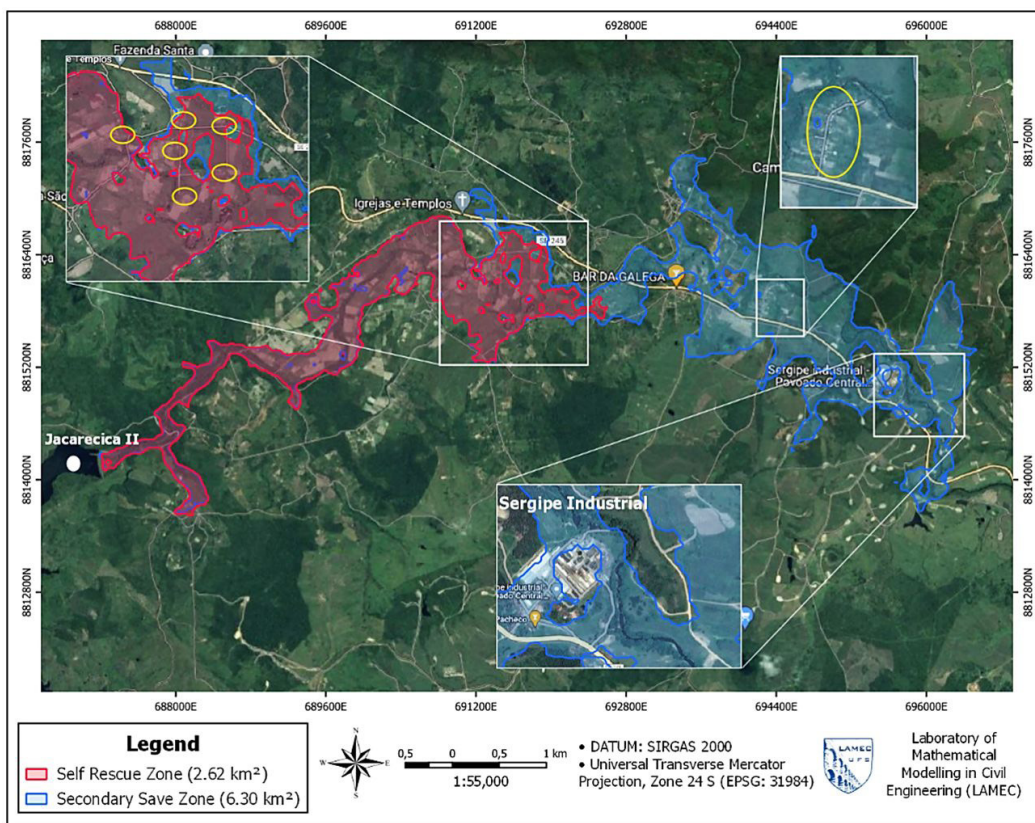


Figure 9. SRZ and SSZ delimitation for sunny day extreme rupture scenario.

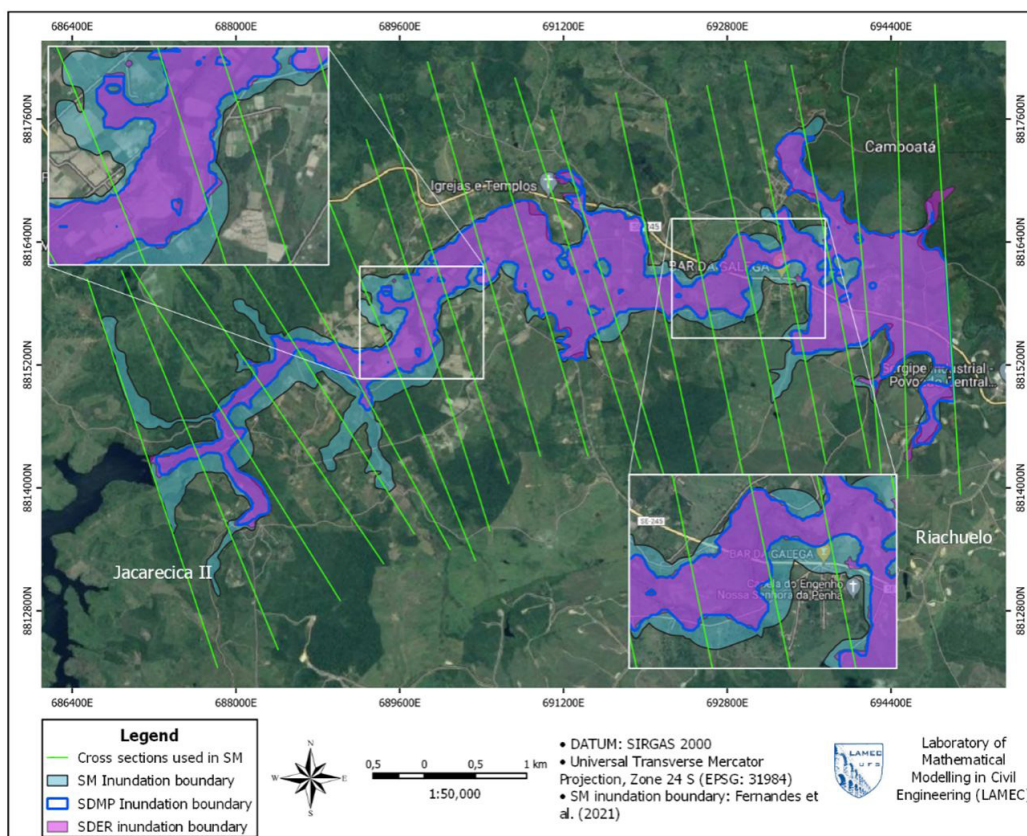


Figure 10. Inundation boundaries obtained from Simplified Methodology (SM), sunny day most probable (SDMP) and sunny day extreme rupture (SDER) scenarios.

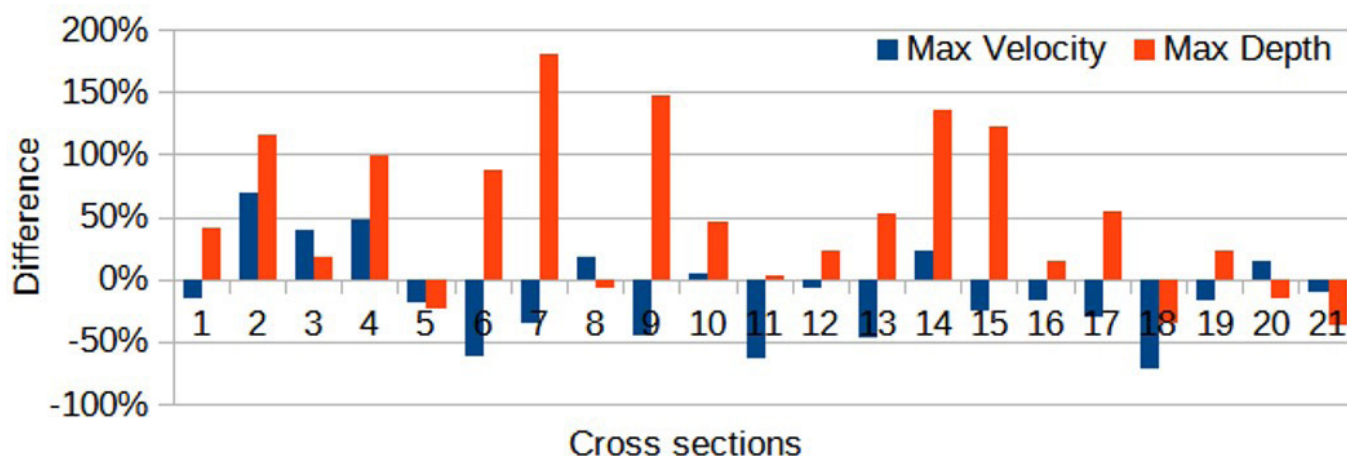


Figure 11. Percentual differences between maximum velocity and depth obtained from SM and HR model outputs for sunny day most probable rupture scenario (SDMP).

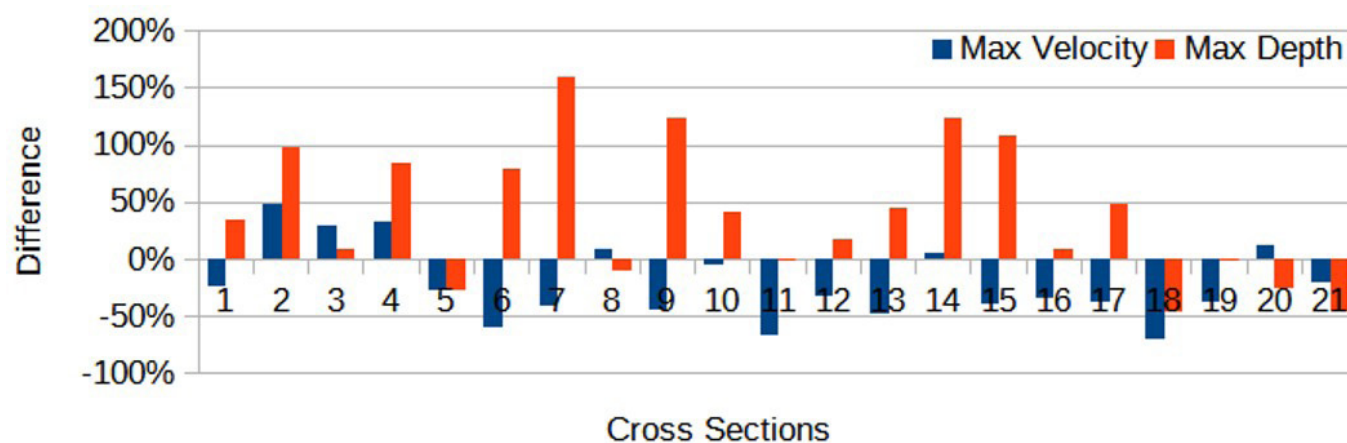


Figure 12. Percentual differences between maximum velocity and depth obtained from SM and HR model outputs for sunny day extreme rupture scenario (SDER).

Even though it was expected that the SM would result in greater maximum flows, it is important to enlighten that the methodology was designed for dams associated potential damage classification, not for detailed dam break studies (Agência Nacional de Águas e Saneamento Básico, 2017).

CONCLUSIONS

The present work simulated the propagation of the flood wave due to hypothetical ruptures of Jacarecica I and Jacarecica II dams, using the 2D HEC-RAS (HR) hydrodynamic model. To the best of our knowledge, this is the first work that addresses an hypothetical dam break simulation using hydrodynamic modelling in dams located in Sergipe. Since the National Dam Safety Policy require the development of dam safety plans, which includes inundation studies, for the structures, the importance of the work is paramount.

According to the simulation results, maximum depths and velocities of 10 m and 4,5 m.s⁻¹ were registered, and the flood waves take minimal time of 6 to 8 hours to reach Riachuelo,

the closest city downstream of the dams. Within the Self Rescue Zones delimited it was located agricultural land, villages, isolated households and transportation infrastructure, which alerts to the need of an immediate Emergency Acting Plan (EAP) development for the studied structures.

The comparison between HR and Simplified Methodology (SM) results revealed the already suspected conclusion: the SM overestimates maximum flow through the breach and along the downstream valley, as it considers total dam body failure and doesn't account for floodplain roughness and river meanders, which naturally dampen any water flow. Regarding the inundation boundaries, both HR and SM results showed similar morphology, indicating adequacy to predict the spatial coverage of the flood.

Even though important results were obtained in this research, their main limitations are due to the uncertainty amongst data input in the HR model: (i) the only available DEM's low spatial resolution (30 m, adequate to regional studies, but limited for more precise/local studies); (ii) the breach geometries and formation time (parameters considered from literature); (iii) the definition of flow resistance parameters (average Manning Coefficients);

and (iv) and the nonexistence of fluvimetric gauges within the studied area (leading to inadequate calibration of hydrological model). Despite these limitations, the use of high-resolution optical satellite images allowed a good assessment on the actual land cover in the region, which led to a detailed average Curve Number calculation and Manning's Coefficients attribution).

Potential developments and further steps of the study should address better ways to calibrate hydrological and hydraulic models, i. e. using in-site flow measurements and/or regionalization methods. Furthermore, the usage of a more precise DEM, i.e. LiDAR-derived, would result in a more precise prediction of the dam break wave propagation. Besides these factors, the results obtained with the available data have enlightened the need for better dam safety actions in Sergipe state.

ACKNOWLEDGEMENTS

The authors would like to thank the Water Resources Development and Irrigation Company of Sergipe (COHIDRO) and the Special Superintendence for Water Resources and Environment of Sergipe (SERHMA-SE) for the support provided for this research to be conducted.

REFERENCES

- Abdi, A. M. (2020). Land cover and land use classification performance of machine learning algorithms in a boreal landscape using Sentinel-2 data. *GIScience & Remote Sensing*, 57(1), <http://dx.doi.org/10.1080/15481603.2019.1650447>.
- Acharki, S. (2022). PlanetScope contributions compared to Sentinel-2, and Landsat-8 for LULC mapping. *Remote Sensing Applications: Society and Environment*, 27, <http://dx.doi.org/10.1016/j.rsase.2022.100774>.
- Acharki, S., Frison, P. L., Amharref, M., Khoj, H., Bernoussi, S. (2021). Complementarity of sentinel-2 optical images with radar images (sentinel-1 and alos-palsar-2) for plant cover mapping: application to a protected area and its surroundings in northwestern Morocco via three machine learning algorithms. *ISPRS Journal of Photogrammetry and Remote Sensing*, 223, 143-158. <http://dx.doi.org/10.52638/rfpt.2021.599>.
- Agência Nacional de Águas e Saneamento Básico – ANA. (2016). *Guia de orientação e formulários do Plano de Ação de Emergência – PAE*. (In Portuguese). Retrieved in 2023, May 25, from <https://bit.ly/3EUSQXJ> [Q3: Q3]].
- Agência Nacional de Águas e Saneamento Básico – ANA. (2017). *Geração de Manchas para a Classificação de Barragens quanto ao Dano Potencial Associado*. (In Portuguese). Retrieved in 2023, May 25, from https://www.snirh.gov.br/portal/snirh/Entenda_Mais/capacitacao/Arquivos_Cursos/treinamento-sobre-metodologia-simplificada-para-definicao-da-mancha-de-classificacao-do-dano-potencial-associado-dpa-da-baragem
- Agência Nacional de Águas e Saneamento Básico – ANA. (2021). *Painel de informações do SNISB*. (In Portuguese). Retrieved in 2023, May 25, from <https://bit.ly/3hmo9zz>.
- Alizadeh, Z., & Yazdi, J. (2023). Calibration of hydrological models for ungauged catchments by automatic clustering using a differential evolution algorithm: the Gorganrood river basin case study. *Journal of Hydroinformatics*, 25(3), 645-662. <http://dx.doi.org/10.2166/hydro.2023.081>.
- Álvarez, M., Puertas, J., Peña, E., & Bermúdez, M. (2017). Two-dimensional dam-break flood analysis in data-scarce regions: the case study of Chipembe Dam, Mozambique. *Water (Basel)*, 9(6), 432. <http://dx.doi.org/10.3390/w9060432>.
- Amini, A., Bahrami, J., & Miraki, A. (2022). Effects of dam break on downstream dam and lands using GIS and Hec Ras: a decision basis for the safe operation of two successive dams. *International Journal of River Basin Management*, 20(4), 487-498. <http://dx.doi.org/10.1080/15715124.2021.1901728>.
- Aragão, R., Santana, G. R., Costa, C. E. F. F., Cruz, M. A. S., Figueiredo, E. E., & Srinivasan, V. (2013). Chuvas intensas para o Estado de Sergipe com base em dados desagregados de chuva diária. *Revista Brasileira de Engenharia Agrícola e Ambiental*, 17(3), 243-252. <http://dx.doi.org/10.1590/S1415-43662013000300001>.
- Aragon, B., Ziliani, M. G., Houborg, R., Franz, T. E., & McCabe, M. F. (2021). CubeSats deliver new insights into agricultural water use at daily and 3 m resolutions. *Scientific Reports*, 11, 12131. <http://dx.doi.org/10.1038/s41598-021-91646-w>.
- Armada, C. A. S. (2021). Os desastres ambientais de Mariana e Brumadinho em face ao estado socioambiental brasileiro. *Territorium*, 28(I), 13-22. http://dx.doi.org/10.14195/1647-7723_28-1_1.
- Azevedo, R. L., & Sousa, I. F. (2020). Classificação climática da bacia hidrográfica do rio Jacarecica. In C. A. B. Garcia, I. F. Sousa, A. S. C. Monteiro & N. R. F. Santana (Eds.), *Caracterização ambiental e hidrológica da bacia hidrográfica do rio Jacarecica* (pp. 26-34). Belo Horizonte, MG: Editora Poisson.
- Aziz, K. M. A., & Rashwam, K. S. (2022). Comparison of different resolutions of six free online DEMs with GPS elevation data on a new 6th of October City, Egypt. *Arabian Journal of Geosciences*, 15, 1585. <http://dx.doi.org/10.1007/s12517-022-10845-5>.
- Azizian, A., & Brocca, L. (2020). Determining the best remotely sensed DEM for flood inundation mapping in sparse regions. *International Journal of Remote Sensing*, 41(5), 1884-1906. <http://dx.doi.org/10.1080/01431161.2019.1677968>.
- Barbosa, A. G., Celeste, A. B., & Mendes, L. A. (2021). Influence of inflow nonstationarity on the multipurpose optimal operation of hydropower plants using nonlinear programming. *Water Resources Management*, 35, 2343-2367. <http://dx.doi.org/10.1007/s11269-021-02812-8>.
- Bellos, V., Tsakiris, V. K., Kopsiaftis, G., & Tsakiris, G. (2020). Propagating dam breach parametric uncertainty in a river reach using the HEC-RAS software. *Hydrology*, 7(4), 72. <http://dx.doi.org/10.3390/hydrology7040072>.

- Brasil. Diretoria de Planejamento e Pesquisa. Coordenação Geral de Estudos e Pesquisa. Instituto de Pesquisas Rodoviárias. Departamento Nacional de Infraestrutura de Transportes - DNIT. (2005). *Manual de hidrologia básica para estruturas de drenagem* (2. ed.). Rio de Janeiro: IPR Publ. (In Portuguese).
- Campos, R. G. D., Saliba, A. P. M., Baptista, M. B., Biscaro, V. H. B., Miranda Sá, J. M., Passos, D. T., Coelho, S. A. S., & Gomez, J. A. M. (2020). Breach parameters for cascade dams' breaks using physical, empirical and numerical modeling. *Revista Brasileira de Recursos Hídricos*, 25, e30. <http://dx.doi.org/10.1590/2318-0331.252020190109>.
- Carrera-Hernández, J. J. (2021). Not all DEMs are equal: an evaluation of six globally available 30 m resolution DEMs with geodetic benchmarks and LiDAR in Mexico. *Remote Sensing of Environment*, 261, <http://dx.doi.org/10.1016/j.rse.2021.112474>.
- Chow, V. T. (1959). *Open-Channel Hydraulics*. McGraw-Hill. New York.
- Courty, L. G., Soriano-Monzalvo, J. C., & Pedrozo-Acuña, A. (2019). Evaluation of open-access global digital elevation models (AW3D30, SRTM, and ASTER) for flood modelling purposes. *Journal of Flood Risk Management*, 12, <http://dx.doi.org/10.1111/jfr3.12550>.
- Degraf, H., & Detzel, D. H. M. (2022). Influence of nonstationarity on reservoir storage-yield-reliability relationships. *Revista Brasileira De Recursos Hídricos*, 27, e35. <http://dx.doi.org/10.1590/2318-0331.272220220043>.
- Federal Emergency Management Agency – FEMA. (2013). *Federal Guidelines for Dam Safety: Emergency Action Planning for Dams. Report FEMA n. 64, July 2013*. Retrieved in 2023, July 20, from <https://tinyurl.com/msuhhbm>.
- Fernandes, M. R. D. M., Souza, T. P. D., Rocha, J. C. S. D., Macedo, A. P. B. A., & Souza, R. G. D. (2021). Simulação da mancha de inundação do rompimento hipotético da barragem Jacareica II, Sergipe. In *XIII Encontro de Recursos Hídricos em Sergipe*, Aracaju-SE, 22 a 24 de março de 2021. Retrieved in 2023, May 25, from <https://anais.abrhidro.org.br/job.php?Job=6577>
- Fleischmann, A., Paiva, R., & Collischonn, W. (2019). Can regional to continental river hydrodynamic models be locally relevant? A cross-scale comparison. *Journal of Hydrology: X*, 3, 100027. <http://dx.doi.org/10.1016/j.hydroa.2019.100027>.
- Franks, S., Storey, J., & Rengarajan, R. (2020). The new landsat collection-2 digital elevation model. *Remote Sensing*, 12, 3909-3932. <http://dx.doi.org/10.3390/rs12233909>.
- Froehlich, D. C. (1995). Peak outflow from breached embankment dam. *Journal of Water Resources Planning and Management*, 121(1), [http://dx.doi.org/10.1061/\(ASCE\)0733-9496\(1995\)121:1\(90\)](http://dx.doi.org/10.1061/(ASCE)0733-9496(1995)121:1(90)).
- Froehlich, D. C. (2008). Embankment dam breach parameters and their uncertainties. *Journal of Hydraulic Engineering (New York, N.Y.)*, 134(12), [http://dx.doi.org/10.1061/\(ASCE\)0733-9429\(2008\)134:12\(1708\)](http://dx.doi.org/10.1061/(ASCE)0733-9429(2008)134:12(1708)).
- García, M., Juan, A., & Bedient, P. (2020). Integrating reservoir operations and flood modeling with HEC-RAS 2D. *Water (Basel)*, 12(8), 2259. <http://dx.doi.org/10.3390/w12082259>.
- Garg, R., Kumar, A., Prateek, M., Prateek, M., & Kumar, S. (2022). Land cover classification of spaceborne multifrequency SAR and optical multispectral data using machine learning. *Advances in Space Research*, 69(4), 1726-1742. <http://dx.doi.org/10.1016/j.asr.2021.06.028>.
- Garooosi, F., Mellado-Cusichua, A. N., Shademani, M., & Shakibaeinia, A. (2022). Experimental and numerical investigations of dam break flow over dry and wet beds. *International Journal of Mechanical Sciences*, 215, <http://dx.doi.org/10.1016/j.ijmecsci.2021.106946>.
- Ge, W., Jiao, Y., Wu, M., Li, Z., Zhang, Y., Wang, T., Li, W., Gao, W., & Gelder, P. (2022). Estimating loss of life caused by dam breaches based on the simulation of floods routing and evacuation potential of population at risk. *Journal of Hydrology (Amsterdam)*, 612, 128059.
- Gonçalves, D. N., Junior, J. M., Carrilho, A. C., Acosta, P. R., Ramos, A. P. M., Gomes, F. D. G., Osco, L. P., Oliveira, M. R., Martins, J. A. C., Júnior, G. A. D., Araújo, M. S., Li, J., Roque, F., Peres, L. F., Gonçalves, W. N., Libonati, R. (2023). Transformers for mapping burned areas in Brazilian Pantanal and Amazon with PlanetScope imagery. *International Journal of Applied Earth Observation and Geoinformation*, 116, <http://dx.doi.org/10.1016/j.jag.2022.103151>.
- Guimarães, R. N., Moreira, V. R., Cruz, J. R. A., Saliba, A. P. M., & Amaral, M. C. S. (2022). History of tailings dam failure: impacts on access to safe water and influence on the legislative framework. *The Science of the Total Environment*, 852, <http://dx.doi.org/10.1016/j.scitotenv.2022.158536>.
- Haltas, I., Tayfur, G., & Elci, S. (2016). Two-dimensional numerical modeling of flood wave propagation in an urban area due to U˘rkmez dam-break, Izmir, Turkey. *Natural Hazards*, 81(3), 2103-2119. <http://dx.doi.org/10.1007/s11069-016-2175-6>.
- Hosseinzadeh-Tabrizi, S. A., Ghaeini-Hessaroeeyeh, M., & Ziaadini-Dashtekhaki, M. (2022). Numerical simulation of dam-breach flood waves. *Applied Water Science*, 12(100), <http://dx.doi.org/10.1007/s13201-022-01623-5>.
- Hu, L. M., Yang, X., Li, Q., & Li, S. Y. (2020). Numerical simulation and risk assessment of cascade reservoir dam-break. *Water (Basel)*, 12(6), 1730. <http://dx.doi.org/10.3390/w12061730>.
- Isensee, L. J., Pinheiro, A., & Detzel, D. H. M. (2021). Dam hydrological risk and the design flood under non-stationary conditions. *Water Resources Management*, 35, 1499-1512. <http://dx.doi.org/10.1007/s11269-021-02798-3>.
- Kanani-Sadat, Y., Arabsheibani, R., Karimipour, F., & Nasser, M. (2019). A new approach to flood susceptibility assessment in data-scarce and ungauged regions based on GIS-based hybrid multi criteria decision-making method. *Journal of Hydrology (Amsterdam)*, 572, 17-31. <http://dx.doi.org/10.1016/j.jhydrol.2019.02.034>.

- Koch, H., Silva, A. L. C., Liersch, S., Azevedo, J. R. G., & Hattermann, F. F. (2020). Effects of model calibration on hydrological and water resources management simulations under climate change in a semi-arid watershed. *Climatic Change*, *163*, 1247-1266. <http://dx.doi.org/10.1007/s10584-020-02917-w>.
- Leach, N., Coops, N. C., & Obrknezev, N. (2019). Normalization method for multi-sensor high spatial and temporal resolution satellite imagery with radiometric inconsistencies. *Computers and Electronics in Agriculture*, *164*, <http://dx.doi.org/10.1016/j.compag.2019.104893>.
- Lopes, M., Frison, P. L., Crowson, M., Warren-Thomas, E., Hariyadi, B., Kartika, W. D., Agus, F., Hamer, K. C., Stringer, L., Hill, J. K., & Pettorelli, N. (2020). Improving the accuracy of land cover classification in cloud persistent areas using optical and radar satellite image time series. *Methods in Ecology and Evolution*, *11*, 532-541. <http://dx.doi.org/10.1111/2041-210X.13359>.
- Maxwell, A. E., Warner, T. A., & Fang, F. (2018). Implementation of machine-learning classification in remote sensing: an applied review. *International Journal of Remote Sensing*, *39*(9), 2784-2817. <http://dx.doi.org/10.1080/01431161.2018.1433343>.
- McClellan, F., Dawson, R., & Kilsby, C. (2020). Implications of using global digital elevation models for flood risk analysis in cities. *Water Resources Research*, *56*(10), <http://dx.doi.org/10.1029/2020WR028241>.
- Mei, S., Zhong, Q., Yang, M., Chen, S., Shan, Y., & Zhang, L. (2023). Overtopping-Induced breaching process of concrete-faced rockfill dam: a case study of Upper Taum Sauk dam. *Engineering Failure Analysis*, *144*, <http://dx.doi.org/10.1016/j.engfailanal.2022.106982>.
- Moglen, G. E., Sadeq, H., Hughes, L. H., Meadows, M. E., Miller, J. J., Ramirez-Aviles, J. J., & Tollner, E. W. (2022). NRCS curve number method: comparison of methods for estimating the curve number from rainfall-runoff data. *Journal of Hydrologic Engineering*, *27*(10), 04022023.
- Mohanty, M. P., Nithya, S., Akhilesh, S., Indu, J., Ghosh, S., Bhatt, C. M., Rao, G. S., & Karmakar, S. (2020). Sensitivity of various topographic data in flood management: implications on inundation mapping over large data-scarce regions. *Journal of Hydrology (Amsterdam)*, *590*, <http://dx.doi.org/10.1016/j.jhydrol.2020.125523>.
- Mudashiru, R. B., Sabtu, N., Abustan, I., & Balogun, W. (2021). Flood hazard mapping methods: a review. *Journal of Hydrology (Amsterdam)*, *603*, 126846.
- Nagel, G. W., Novo, E. M. L. M., & Kampel, M. (2020). Nanosatellites applied to optical Earth observation: a review. *Ambiente & Água*, *15*(3), <http://dx.doi.org/10.4136/ambi-agua.2513>.
- National Aeronautics and Space Administration-Jet Propulsion Laboratory – NASA-JPL. (2021). *NASADEM Merged DEM Global 1 arc second. [NASADEM_HGT v001]*. NASA EOSDIS Land Processes DAAC. Retrieved in 2023, July 20, from https://lpdaac.usgs.gov/products/nasadem_hgtv001/
- Ongdas, N., Akiyanova, F., Karakulov, Y., Muratbayeva, A., & Zinabdin, N. (2020). Application of HEC-RAS (2D) for Flood Hazard Maps Generation for Yesil (Ishim) River in Kazakhstan. *Water (Basel)*, *12*(10), 2672. <http://dx.doi.org/10.3390/w12102672>.
- Ouarda, T. B. M. J., Latifa, A. Y., & Christian, C. (2019). Non-stationary intensity-duration-frequency curves integrating information concerning teleconnections and climate change. *International Journal of Climatology*, *39*(4), 2306-2323. <http://dx.doi.org/10.1002/joc.5953>.
- Pereira, C. E., Viseu, M. T., Melo, J. F., Martins, T., Salla, M. R., & Mota, K. R. R. (2017). Comparação entre modelos simplificados e o modelo HEC-RAS no estudo de áreas de inundação para o caso de Minas Gerais, Brasil. *Revista Brasileira de Recursos Hídricos*, *38*(1), 75-90. <http://dx.doi.org/10.5894/rh38n1-cti3>.
- Pinheiro, V. B., Naghettini, M., & Palmier, L. R. (2019). Uncertainty estimation in hydrodynamic modeling using Bayesian techniques. *Revista Brasileira de Recursos Hídricos*, *24*(e38), <http://dx.doi.org/10.1590/2318-0331.241920180110>.
- Planet Team. (2021). *Planet Imagery Product Specifications*. Retrieved in 2023, July 20, from <https://bit.ly/2UqRWi5>.
- Poursanidis, D., Traganos, D., Chrysoulakis, N., & Reinartz, P. (2019). Cubesats allow high spatiotemporal estimates of satellite-derived bathymetry. *Remote Sensing*, *11*, 1299. <http://dx.doi.org/10.3390/rs11111299>.
- Rocha, S. L., & Almeida, J. A. P. (2020). Análise morfológica da bacia hidrográfica do rio Jacarecica, no estado de Sergipe, utilizando o aplicativo Archydro. In C. A. B. Garcia, I. F. Sousa, A. S. C. Monteiro, & N. R. F. Santana (Eds.), *Caracterização ambiental e hidrológica da bacia hidrográfica do rio Jacarecica* (pp. 8-25). Belo Horizonte, MG: Editora Poisson.
- Rolo, R. M., Marodin, F. A., Carrard, G. P., Cardone, L. B., & Silveira, C. J. S. (2023). A Python implementation for the simplified dam-break flood modeling. *Revista Brasileira de Recursos Hídricos*, *27*, <http://dx.doi.org/10.1590/2318-0331.272220220013>.
- Sartori, A., Neto, F., & Genovez, A. (2005). Classificação hidrológica de solos brasileiros para estimativa da chuva excedente com o método do serviço de conservação do solo dos Estados Unidos Parte 1: classificação. *Revista Brasileira de Recursos Hídricos*, *10*(4), 5-18. <http://dx.doi.org/10.21168/rbrh.v10n4.p5-18>.
- Schumann, G. J. P., Brakenridge, G. R., Kettner, A. J., Kashif, R., & Niebur, E. (2018). Assisting flood disaster response with earth observation data and products: a critical assessment. *Remote Sensing*, *10*, 1230. <http://dx.doi.org/10.3390/rs10081230>.
- Sergipe. Secretaria de Estado do Meio Ambiente e dos Recursos Hídricos de Sergipe - SEMARH-SE. Unidade Técnica de Administração do Programa Águas de Sergipe – UAPAS. (2015). *Relatório técnico de segurança de barragens*. (In Portuguese). Retrieved in 2023, May 25, from <https://1drv.ms/b/s!Ahh1ButW0ENLgdM2EU2o8tRvKltpQ?e=EVMG2h>.

- Sergipe. Secretaria de Estado do Desenvolvimento Urbano e Sustentabilidade de Sergipe – SEDURBS-SE. Secretaria de Recursos Hídricos – SRH. (2012). *Atlas digital sobre recursos hídricos de Sergipe: base de dados geoespacial*. Sergipe: SRH. (In Portuguese).
- Sergipe. Secretaria de Estado do Meio Ambiente e dos Recursos Hídricos de Sergipe – SEMARH-SE. Unidade Técnica de Administração do Programa Águas de Sergipe – UAPAS. (2018). *Serviços de batimetria nos reservatórios das barragens Jacareica I, Jacareica II e Governador João Alves Filho: Relatório Técnico do serviço executado pela empresa CHD - Cartografia, Hidrografia e Digitalização Ltda*. Retrieved in 2023, May 25, from https://1drv.ms/b/s!AghiButW0ENLg4zJ__1TS8tv0gJPw?e=oaxlte
- Sergipe. Secretaria Estadual de Meio Ambiente e dos Recursos Hídricos – SEMARH. Consórcio TECHNE-ENGEVIX. (2019). *Consultoria para a elaboração de estudos hidrológicos nas bacias hidrográficas das barragens Jacareica I, Jacareica II e Governador João Alves Filho. Produto 7 – Estudo Hidrológico do Reservatório Jacareica I*. Retrieved in 2023, May 25, from <https://1drv.ms/b/s!AghiButW0ENLgdgeXe6Cs4g5U3R2Yw?e=SNmjZH>
- Souza Junior, C. M., Shimbo, J. Z., Rosa, M. R., Parente, L. L., Alencar, A. A., Rudorff, B. F. T., Hasenack, H., Matsumoto, M., Ferreira, L. G., Souza-Filho, P. W. M., Oliveira, S. W., Rocha, W. F., Fonseca, A. V., Marques, C. B., Diniz, C. G., Costa, D., Monteiro, D., Rosa, E. R., Velez-Martin, E., Weber, E. J., Lenti, F. E. B., Paternost, F. F., Pareyn, F. G. C., Siqueira, J. V., Vieira, J. L., Ferreira Neto, L. C., Saraiva, M. M., Sales, M. H., Salgado, M. P. G., Vasconcelos, R., Galano, S., Mesquita, V. V., & Azevedo, T. (2020). Reconstructing three decades of land use and land cover changes in Brazilian biomes with Landsat archive and Earth Engine. *Remote Sensing*, 12(17), 2735. <http://dx.doi.org/10.3390/rs12172735>.
- Tschiedel, A. F., & Paiva, R. C. D. (2018). Uncertainty assessment in hydrodynamic modeling of floods generated by dam break. *Revista Brasileira de Recursos Hídricos*, 23, e30. <http://dx.doi.org/10.1590/2318-0331.231820170074>.
- Tschiedel, A. F., Paiva, R. C. D., & Fan, F. M. (2020). Use of large-scale hydrological models to predict dam break-related impacts. *Revista Brasileira de Recursos Hídricos*, 25(35). <http://dx.doi.org/10.1590/2318-0331.252020190128>.
- Tu, Y. H., Johansen, K., Aragon, B., El Hajj, M. M., & McCabe, M. F. (2022). The radiometric accuracy of the 8-band multi-spectral surface reflectance from the planet SuperDove constellation. *International Journal of Applied Earth Observation and Geoinformation*, 114, <http://dx.doi.org/10.1016/j.jag.2022.103035>.
- United States Army Corps of Engineers – USACE. (2021). *HEC-RAS River Analysis System: User's Manual. Version 6.0. Institute for Water Resources. Hydrologic Engineering Center (HEC). Report n. CPD-68*. Retrieved in 2023, May 25, from https://www.hec.usace.army.mil/software/hec-ras/documentation/HEC-RAS_6.0_Users_Manual.pdf
- Uuemaa, E., Ahi, S., Montibeller, B., Muru, M., & Kmoh, A. (2020). Vertical accuracy of freely available global digital elevation models (ASTER, AW3D30, MERIT, TanDEM-X, SRTM, and NASADEM). *Remote Sensing*, 12, 3482. <http://dx.doi.org/10.3390/rs12213482>.
- Vieira, L. M. S., Fontes, A. S., & Simões, A. L. A. (2019). Analysis of physical mechanisms of human body instability for the definition of hazard zones present in emergency action plans of dams. Case study: Santa Helena Dam, Bahia. *Revista Brasileira de Recursos Hídricos*, 24, <http://dx.doi.org/10.1590/2318-0331.241920180185>.
- Von Thun, J. L., & Gillette, D. R. (1990). *Guidance on breach parameters*. Denver, Colorado: U.S. Bureau of Reclamation.
- Wambugu, N., Chen, Y., Xiao, Z., Tan, K., Wei, M., Liu, X., & Li, J. (2021). Hyperspectral image classification on insufficient-sample and feature learning using deep neural networks: A review. *International Journal of Applied Earth Observation and Geoinformation*, 105, <http://dx.doi.org/10.1016/j.jag.2021.102603>.
- Xavier, A. C., King, C. W., & Scanlon, B. R. (2016). Daily gridded meteorological variables in Brazil (1980-2013). *International Journal of Climatology*, 36(6), 2644-2659. <http://dx.doi.org/10.1002/joc.4518>.
- Zhang, K., Gann, D., Ross, M., Robertson, Q., Sarmiento, J., Santana, S., Rhome, J., & Fritz, C. (2019). Accuracy assessment of ASTER, SRTM, ALOS, and TDX DEMs for Hispaniola and implications for mapping vulnerability to coastal flooding. *Remote Sensing of Environment*, 225, 290-306. <http://dx.doi.org/10.1016/j.rse.2019.02.028>.
- Zhong, Q., Wang, L., Chen, S., Chen, Z., Shan, Y., Zhang, Q., Ren, Q., Mei, S., Jiang, J., Hu, L., & Liu, J. (2021). Breaches of embankment and landslide dams: state of the art review. *Earth-Science Reviews*, 216, <http://dx.doi.org/10.1016/j.earscirev.2021.103597>.

Authors contributions

Leonardo de Carvalho Souza Santa Rita: Methodology definition, hydrological analysis, modeling and simulation, results analysis, article writing.

Abraão Nunes de Oliveira: Statistical procedures, hydrological analysis, modeling and simulation.

André Quintão de Almeida: Methodology definition, results analysis, article writing, supervision.

Ludmilson Abritta Mendes: Methodology definition, results analysis, article writing, supervision.

Editor in-Chief: Adilson Pinheiro

Associated Editor: Iran Eduardo Lima Neto